



Energy, exergy, sustainability, environmental emission, and fuel cost analysis of a hot-dip galvanised steel wire process

T. Álvarez-Álvarez ^a, A. Barbón ^b, L. Bayón ^c,* , C.A. Silva ^d

^a Polytechnic School of Engineering of Gijón, University of Oviedo, Spain

^b Department of Electrical Engineering, University of Oviedo, Spain

^c Department of Mathematics, University of Oviedo, Spain

^d Center for Innovation, Technology and Policy Research, Instituto Superior Tecnico, University of Lisbon, Portugal

ARTICLE INFO

Keywords:

Hot-dip galvanised steel wire process
Aspen HYSYS model
Computational fluid dynamics model
Energy analyses
Exergy analyses
Sustainability analyses

ABSTRACT

Hot-dip galvanised steel is a widely used process to protect metals from corrosion. This process is considered an energy-intensive and highly polluting industry. In this context, the present study aims to investigate an energy, exergy, sustainability, environmental emissions and fuel cost analysis of a hot-dip galvanised steel wire process. For this purpose, a real hot-dip galvanised steel wire process belonging to the company Moreda Riviere Trefilerías S.A. (Spain) has been analysed. The parameters necessary to perform the thermodynamic analysis are obtained by means of process models. The methodology used comprises the following steps: a process analysis, an experimental setup, a modelling of the flue gases using the Aspen HYSYS model, a modelling of the galvanising barrel using the computational fluid dynamics model, and a validation of the process. The following conclusions can be drawn from the results: (i) The energy efficiency of the system, burners and galvanising barrel is 62.11%, 42.36% and 34.27%, respectively; (ii) The exergy efficiency of the system, burners and galvanising barrel is 90.84%, 78.90% and 56.60%, respectively; (iii) The sustainability index is 10.92; (iv) The galvanising process emits 72.61 (kg/h) CO₂, i.e. 636.06 (t) CO₂ per year. Therefore, galvanising 1 (kg) of wire in the actual process emits 0.0348 (kg) of CO₂; and (v) The natural gas consumption is 25.67 (kg/h), i.e. 224.87 (t) of natural gas per year. Therefore, galvanising 1 (kg) of wire requires 0.0123 (kg) of natural gas. These results invite to study, in future work, the possibility of including other technologies, such as cogeneration systems, the use of new burner arrangements, hydrogen-enriched natural gas, solar thermal energy and photovoltaic systems.

1. Introduction

Steel is a material that is used in a multitude of sectors, such as industrial construction, industrial machinery, automotive industry, housing, etc [1]. The construction of buildings, bridges, high-rise structures, etc. are typical applications of structural steel. There are several reasons for this widespread use, such as: (i) its cost-effectiveness, (ii) its strength, (iii) its versatility, (iv) its portability, and (v) its recyclability. Due to these characteristics, world crude steel production was 1,849.7 million tonnes (Mt) in 2023, according to a report by the World Steel Association [2]. China accounted for 55.09% of all global production and the European Union for 6.83%. However, their use in outdoor projects and other harsh environments is affected by the phenomenon of corrosion. Standardising the corrosion process that occurs in bare steel is extremely complex, as it is influenced by several parameters that are difficult to standardise, such as [3]: variation in the composition/structure of the steel, the presence of impurities due to the

use of recycled steel, uneven internal stresses, the type of installation environment, etc.

In 2013, the global cost of corrosion was estimated to be 3.4% of global GDP (Gross Domestic Product) [4]. That is, US\$2.5 trillion [4] of direct cost. Moreover, these costs did not include aspects related to safety (accidents, near misses, incidents, etc.), to indirect cost (production interruption, forced shutdowns), and to the environment. It has been estimated that 15 – 35% of the annual cost of corrosion could be saved globally if currently available corrosion control mechanisms were used [4]. i.e. between US\$375 billion and US\$875 billion [4]. For these reasons, it has been established that the lack of corrosion management is very costly because it reduces the lifetime of an asset, and that a corrosion management system is necessary. It is necessary to be aware that corrosion is a natural phenomenon that can be mitigated, but never completely eliminated. However, if appropriate

* Corresponding author.

E-mail address: bayon@uniovi.es (L. Bayón).

<https://doi.org/10.1016/j.energy.2025.134897>

Received 23 June 2024; Received in revised form 29 October 2024; Accepted 5 February 2025

Available online 14 February 2025

0360-5442/© 2025 Elsevier Ltd. All rights are reserved, including those for text and data mining, AI training, and similar technologies.

Nomenclature

C_p	Specific heat (J/kg K)	LTP	Local temperature point (K)
C_p^h	Specific heat for enthalpies (J/mol K)	\dot{m}	Mass flow rate (kg/s)
C_p^s	Specific heat for entropies (J/mol K)	n	Molar flux (mol/s)
E	Energy rate (W)	P	Pressure (kPa)
E_R	Radiant power of each burner (W)	Q	Heat energy rate (W)
E^{ch}	Chemical energy rate (W)	R	Ideal gas constant (J/mol K)
E^{ph}	Physical energy rate (W)	RE	Relative error (%)
E_X	Exergy rate (W)	SI	Sustainability index
E_X^{ch}	Chemical exergy rate (W)	T	Temperature (K)
E_X^{ph}	Physical exergy rate (W)	η	Energy efficiency (%)
h	Enthalpy rates (J/kg)	χ	Mole fraction
LHV	Lower heating value (J/kg)	Ψ	Exergy efficiency rate (%)
		ε_0	Molar chemical exergy (J/mol)

corrosion protection systems, such as hot-dip galvanising, are provided at the start of the project, the above-mentioned cost savings can be achieved, as well as mitigation of the other aspects mentioned. Hot-dip galvanising provides steel wire with three levels of protection from corrosion phenomena [3]: barrier protection, cathodic protection and zinc patina.

Galvanised steel wire is one of the most common types of steel wire due to its properties:

- (i) **Durability.** The development of tightly adhering intermetallic layers is inherent to the hot dip galvanising process, as in the process, a metallurgical reaction takes place between the iron in the steel and the molten zinc in the barrel. These layers are called Gamma, Delta and Zeta, and the top layer of pure zinc, Eta. It is true that the three intermetallic layers are harder than the base steel. While the top layer of pure zinc, Eta, has a ductility that makes it very difficult to damage the coating. These characteristics provide hot-dip galvanised steel with high durability. Because of this property, hot-dip galvanised steel has been widely used in projects located in harsh environments such as: petrochemical, industrial, power generation, bridge construction, etc. Its high abrasion resistance, uniform protection, and that the galvanising process ensures complete coverage, provides protection against damage caused in the assembly process (transportation, handling) of the project, as well as during project operation.
- (ii) **Longevity.** The most demanding atmospheric environments (*UV* rays exposure, snow, submersion or immersion in water, etc.) use galvanised steel for its longevity. The environment determines the corrosion resistance of hot-dip galvanised steel, although it is recognised that it corrodes at 30 times less than bare steel under the same conditions [3]. Several parameters influence the corrosion rate of hot-dip galvanised steel [5]: temperature, humidity, precipitation, sulphur dioxide concentration in the air, and air salinity. Tests have concluded that the time to first maintenance for hot-dip galvanised steels in atmospheric exposure is linear to the thickness of the zinc coating (see Fig. 1). Time to first maintenance is defined as the time to 5% oxidation of the substrate steel [3]. Fig. 1 shows the performance of hot-dip galvanised steel in five environments: industrial, rural, suburban, tropical marine and temperate marine. In this figure, 1 (mil) = 25.4 (μm).
- (iii) **Availability.** The main element in this process is zinc, which occurs naturally in air, soil and water. Moreover, as hot-dip galvanising is a factory-controlled process, it can be carried out 365 days a year, 24 hours a day. As the zinc solidifies as soon as it leaves the vat, without the need for the curing process, the parts can be used immediately.

- (iv) **Versatility.** The hot-dip galvanising process can be applied to parts of different shapes and sizes. For example, nuts, bolts, large fasteners, tubes, etc. As the process involves total immersion of the part, the complete coating of the part is produced.
- (v) **Aesthetics.** There are certain sectors where aesthetics is a highly valued property. Construction projects, bridges, bus stations, property enclosures, etc., the natural grey finish of the hot dip galvanising process gives them an attractive appearance.
- (vi) **Sustainability.** As zinc is naturally occurring in nature it is not harmful to the environment. Moreover, zinc is infinitely recyclable without altering its physico-chemical properties. It is estimated that 30% of the world's zinc supply comes from recycled sources [3].

In 2022, the worldwide Galvanised Steel market was valued at *USD* 162,804.62 million and is projected to grow at a compound annual growth rate of 7.09% until 2028, reaching a total of *USD* 245,612.95 million [6]. The primary consumer of galvanised steel is the energy generation and distribution sector, constituting 40% of the total usage, with building and construction following closely at 25% of the overall production [7]. Additional prevalent applications include road components, industrial equipment, etc. The mounting systems of photovoltaic plants are made of galvanised steel.

The negative aspect of the hot-dip galvanising process is its high energy consumption. Hot-dip galvanised steel wire manufacturing is considered an energy-intensive industry as it is mainly based on combustion processes. Energy-intensive industries are responsible for major environmental and economic impacts. About 85 – 90% of the total energy requirements for the production of hot-dip galvanised steel occur when the zinc melts above 450 ($^{\circ}\text{C}$). During this process, large volumes of flue gas emissions are produced. Typical values for the hot-dip galvanising of 1 (kg) of steel according to UNE-EN ISO 1461 [8] are 0.1 – 0.33 (kg) CO_2 equivalent [9]. Sectors such as steel, chemicals, cement, ceramics, paper, etc. can be included in energy-intensive industries. There are conflicting interests in these industries, on the one hand high energy consumption and on the other hand climate change objectives [10].

The hot-dip galvanising industry is subject to European policies aimed at reducing the greenhouse gas emission (*GGE*) [11–13]. In particular, the European Commission adopted the Roadmap for moving towards a competitive low-carbon economy by 2050 [14], which calls for sectoral strategies to reduce CO_2 emissions by 83 – 87% by 2050 compared to 1990 CO_2 emissions.

Galvanising is a process of coating steel or iron wire with zinc to prevent rusting. The most common practice for galvanising steel wire is hot-dip galvanising [15]. One of the objectives of this study is to analyse in depth the process of hot-dip galvanising of steel wire, as a preliminary step to the decarbonisation of this process by introducing renewable energies into it. The process is carried out by cleaning, fluxing and immersing in a molten zinc bath, which also contains

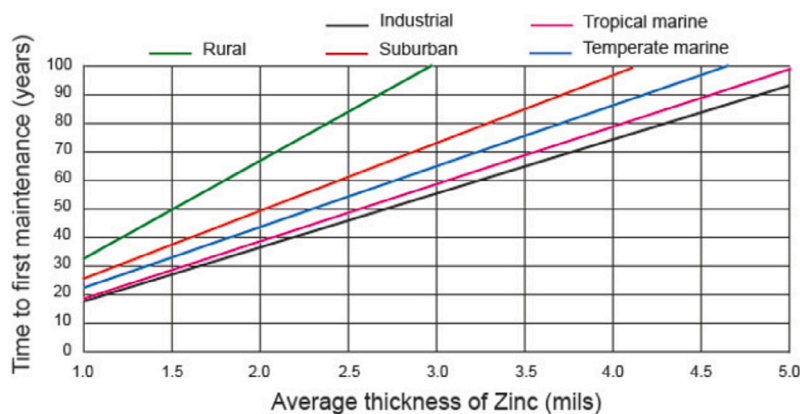


Fig. 1. Time to first maintenance for the galvanised coating.

Table 1

Thermodynamic research studies of industrial processes.

Industrial process	Thermodynamic tool	Env. analysis	Ref.
Ammonia production process	Exergy	Env. assessment	[20]
Fibreglass process	Energy, Exergy	CO ₂ emissions	[21]
Iron and steel industry	Exergy	Emission	[22]
Water desalination process	Energy, Exergy	Env. assessment	[23]
Ceramic industry	Exergy		[24]
Textile industry	Energy, Exergy		[25]
Carob pulp drying system	Energy, Exergy		[26]
Milk transformation process	Energy, Exergy		[27]
Corn grain drying process	Energy, Exergy		[28]

vermiculite on its surface as a thermal insulator, at a temperature that is around 450 (°C), to keep the zinc molten, the wires [1,15].

Blakey and Beck [16] carried out a study to investigate the causes of the high levels of wear of the galvanising barrel walls by means of a model of a hot-dip galvanising furnace using a *CFD* (Computational Fluid Dynamics) model. The values obtained with the model were compared with the values measured in the real process. The results of this comparison show that it is possible to realise a *CFD* model of the galvanising barrel for use in further studies. This study did not present an energy and exergy analysis of the hot-dip galvanising process. Manoj et al. [17] analysed galvanising barrel failures in a hot-dip galvanising process. For this purpose, they used a *CFD* model. They demonstrated that a *CFD* model can be used to simulate the operation of the galvanising barrel. This study did not perform an energy and exergy analysis of the hot dip galvanising process. Dewa et al. [18] presented an analysis of the electrical energy consumed in a hot-dip galvanising process to identify possible actions to reduce electricity consumption. This study did not perform an energy or exergy analysis. Szymczyk and Kluczek [19] presented an analysis of the energy efficiency of a hot-dip galvanising process for steel. This study did not carry out an exergy study of the process, nor a detailed study of the temperature distribution in the galvanising barrel, nor an analysis of the combustion gases. In our paper, we present an energetic and exergetic study, among other studies, of a hot-dip galvanising process. The aim of this work is to fill a technical gap in the analysis of hot-dip galvanising processes.

Several researchers have focused their work on energy, exergy, and environmental analysis of industrial processes, as indicated in Table 1. To our knowledge, there are no studies available in the literature on the energy, exergy, sustainability, and environmental analysis of a hot-dip galvanising process.

The main contributions of this paper can be summarised as follows:

- (i) A proposal of an Aspen HYSYS model of a galvanising process.
- (ii) A computational fluid dynamics modelling of a galvanising process.

- (iii) An energy analysis of a galvanising process.
- (iv) An exergy analysis of a galvanising process.
- (v) A sustainability analysis of a galvanising process.
- (vi) An emissions analysis of a galvanising process.
- (vii) A fuel cost analysis of a galvanising process.
- (viii) An analysis of the potential for the implementation of clean energy in a galvanising process.

Based on the results of the energy and exergy analyses, technologies can be proposed to reduce natural gas consumption, increase process efficiency and reduce CO₂ emissions. The conclusions of this work can help researchers to make decisions and use new approaches on the inclusion of clean energy in the hot-dip galvanising process, to reduce the adverse effects on the environment and to ensure that the industrial process is sustainable.

The paper is organised as follows. Section 2 presents a process analysis. A mathematical formulation of energy, exergy, sustainability and CO₂ emissions is presented in Section 3. In Section 4, a methodology for modelling a hot-dip galvanised steel wire process is proposed. It includes the experimental setup, the modelling of the flue gases using an Aspen HYSYS model, the modelling of the galvanising barrel using a computational fluid dynamics model, and the validation of the modelling. Section 5 presents the results. Section 6 discusses some technologies that could reduce CO₂ emissions and fuel costs. Finally, the conclusions are given in Section 7.

2. Process analysis

The process of hot-dip galvanising steel wire consists of coating steel wire by immersing it in a bath of molten zinc. This process consists of three main steps [3]: (i) surface preparation, (ii) hot-dip galvanising, and (iii) inspection. Step (i), surface preparation, is very important in the application of any coating, as it is common for a coating to fail due to incorrect or inadequate surface preparation. This step consists of: degreasing, pickling and fluxing. In step (ii), i.e. the actual galvanising step of the process, the material is completely immersed in a bath of molten zinc. And in step (iii) the coating thickness and appearance is inspected. In this paper, only step (ii) will be analysed.

The specific case of the hot-dip galvanising of steel wire process analysed is the company Moreda Riviere Trefilerías S.A. [29], located in Gijón (Spain). This company has a 24-wire galvanising line. Fig. 2 shows the 24-wire galvanising line. Number 8 in Fig. 2 indicates where hot-dip galvanising takes place. The most important components of this process are the galvanising barrel, the furnace, and the burners.

The wire used has a diameter between 1.2 and 1.5 (mm), and the operating speeds are 18.7 and 29.2 (m/min) [29], respectively. The thickness of the zinc layer is 20 (µm) [29]. Maximum production of galvanised wire, which passes through the galvanising barrel, is 50

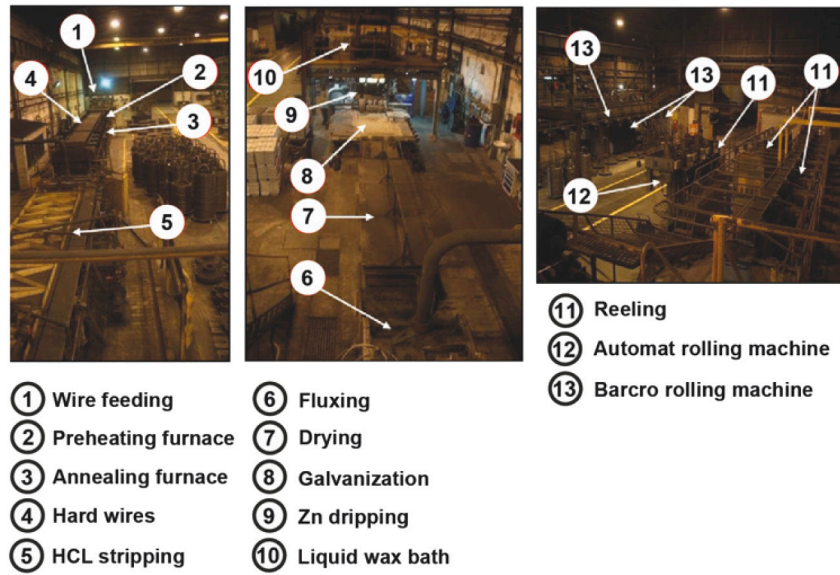


Fig. 2. Installation of the 24-wire galvanising line.

Table 2
Outer dimensions of galvanising barrel and furnace [29].

Component	Width (mm)	Length (mm)	Height (mm)	Thick (mm)
Galvanising barrel	1120	3570	930	50
Furnace	2000	4450	930	200
First floor	2000	4450	170	-
Second floor	2000	4450	170	-

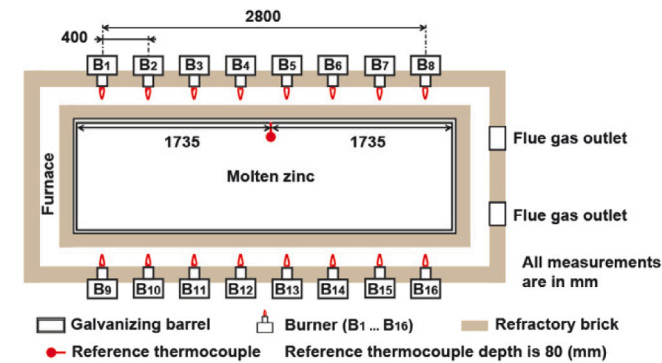


Fig. 3. Schematic of the hot-dip galvanised steel wire system.

(t/day) [29]. The quality of the zinc used is 99.99% Zn (according to the UNE-EN 1179 standard [30]).

The galvanising barrel has a capacity of 20 tonnes of zinc. The galvanising barrel is inserted in a furnace, which has brick walls and a floor made of two layers of concrete. Table 2 summarises the outer dimensions of the galvanising barrel and the furnace.

To prevent the molten zinc from coming into contact with the environment, it is covered with a 40 (mm) thick layer of vermiculite. Therefore, the zinc depth in the barrel is 840 (mm). The combustion equipment consists of 16 burners with a rated output of 90 (kW), model KROMSCHRODER BIO [31], and distributed as indicated in Fig. 3. The burner design allows the mixture of natural gas and air to form the flat flame.

The mode of operation of this process must meet three conditions related to [29]:

- (i) The temperature of the molten zinc (T_{Zn}):

$$T_{Zn} \geq 692.68 \text{ (}^\circ\text{K)} \quad (1)$$

- (ii) The temperature measured by the zinc embedded reference thermocouple (T_{Ref}):

$$745.15 \leq T_{Ref} \leq 757.15 \text{ (}^\circ\text{K)} \quad (2)$$

The reference thermocouple is embedded in the molten zinc, 80 (mm) from the top of the vermiculite layer, i.e. it is embedded in the molten zinc 40 (mm). The location of the reference thermocouple is shown in Fig. 3. The range of values shown in equation (2) is within the typical galvanising temperature (723.15 – 763.15 (°K)) [32].

- (iii) The furnace temperature (T_O):

$$T_O \leq 893.15 \text{ (}^\circ\text{K)} \quad (3)$$

3. Analysis

In this section, the following analyses will be carried out: (i) energy analysis, (ii) exergy analysis, (iii) sustainability analysis, (iv) CO₂ emissions, and (v) fuel cost.

An energy analysis examines the use of energy in the industrial process. For this purpose, energy flows, efficiencies, and losses are examined in order to analyse how energy is used in these industrial processes and to propose strategies for the inclusion of renewable energy systems in energy production.

To assess the quality and usefulness of energy within the industrial process, exergy analysis is used. For this purpose, possible areas for optimisation and improvement of the energy conversion processes are identified by assessing efficiency and exergy losses. This analysis provides information on the thermodynamic performance of the industrial process.

A sustainability analysis of the industrial process will examine various scenarios related to the way in which the necessary energy is obtained.

Environmental emissions associated with industrial processes, such as greenhouse gas emissions and air pollutants, are quantified and

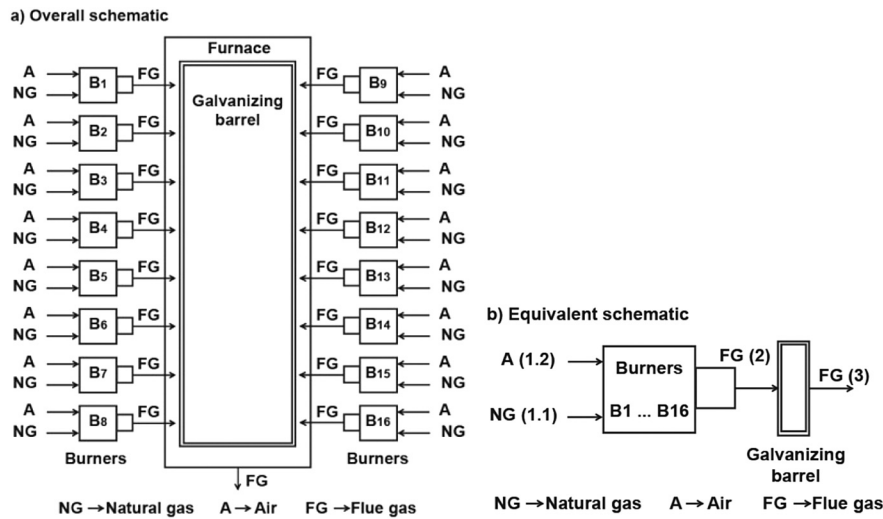


Fig. 4. Overall schematic layout of the actual hot-dip galvanised steel wire process.

assessed in an environmental emissions analysis. Showing the environmental impact of the industrial process is the objective of this type of analysis. This knowledge can guide the inclusion of clean technologies in the industrial process.

The energy, exergy and sustainability analyses of this system are calculated as shown below. Fig. 4 shows the general scheme of the actual hot-dip galvanised steel wire process, containing the main units of this process: (i) sixteen burners, (ii) one galvanising barrel, and (iii) one furnace.

The assumptions made in this study are as follows:

- (i) The entire hot-dip galvanised steel wire system was operated in steady-state [33,34].
- (ii) All gases present in the system, natural gas and flue gas, are considered ideal gas mixtures [34].
- (iii) All combustion reactions are considered complete combustion [34].
- (iv) The electrical energy absorbed by the burners is disregarded due to their low values [34].
- (v) Kinetic and potential energies, and frictional losses are neglected [34].
- (vi) The natural gas and ambient air specifications used in this study are shown in Tables 5 and 6, respectively [34,35].
- (vii) No heat loss in the furnace.

3.1. Energy analysis

The energy analysis is based on the first law of thermodynamics and the mass and energy balance equations. The equation that expresses the energy analysis is as follows [34]:

$$Q_{net,in} + \sum_{in} \dot{m}_{in} \cdot h_{in} = W_{net,out} + \sum_{out} \dot{m}_{out} \cdot h_{out} \quad (4)$$

where $Q_{net,in}$ is the inlet heat energy rate (W), $W_{net,out}$ is the mechanical work output rate (W), h_{in} and h_{out} are the enthalpy input and output rates (J/kg), and \dot{m}_{in} and \dot{m}_{out} are the mass flow input and output rates (kg/s).

3.1.1. Fluids involved in the process

The energy balance equations corresponding to each fluids involved in the process are:

For the natural gas:

Eq. (5) shows the energy balance for natural gas. The energy rate of the natural gas can be calculated as follows [34]:

$$E_{NG} = E_{NG}^{ph} + E_{NG}^{ch} = \dot{m}_{NG} \cdot C_{pNG} \cdot T_{NG} + \dot{m}_{NG} \cdot LHV \quad (5)$$

where E_{NG} is the energy rate of the natural gas (W), E_{NG}^{ph} is the physical energy rate of the natural gas (W), E_{NG}^{ch} is the chemical energy rate of the natural gas (W), \dot{m}_{NG} is the mass flow rate of the natural gas (kg/s), C_{pNG} is the specific heat of the natural gas ($J/kg^\circ K$), T_{NG} is the temperature of the natural gas ($^\circ K$), and LHV is the lower heating value of the natural gas (J/kg).

For the air:

The energy rate of the air can be calculated as follows [34]:

$$E_A = E_A^{ph} = \dot{m}_A \cdot C_{pA} \cdot T_A \quad (6)$$

where E_A is the energy rate of the air (W), E_A^{ph} is the physical energy rate of the air (W), \dot{m}_A is the mass flow rate of the air (kg/s), C_{pA} is the specific heat of the air ($J/kg^\circ K$), and T_A is the temperature of the air ($^\circ K$).

For the flue gases:

In the same way, energy rate is obtained from flue gases [34]:

$$E_{FG} = E_{FG}^{ph} = \dot{m}_{FG} \cdot C_{pFG} \cdot T_{FG} \quad (7)$$

where E_{FG} is the energy rate of the flue gases (W), E_{FG}^{ph} is the physical energy rate of the flue gases (W), \dot{m}_{FG} is the mass flow rate of the flue gases (kg/s), C_{pFG} is the specific heat of the flue gases ($J/kg^\circ K$), and T_{FG} is the temperature of the flue gases ($^\circ K$).

3.1.2. Component of the process

The energy balance equations corresponding to each component of the process are:

For the burners:

The energy balance equation for the burners is (See Fig. 4b):

$$0 = (E_{1.1} + E_{1.2}) - E_2 - E_R \quad (8)$$

where $E_{1.1}$ is the energy input rate of the natural gas in the burners (W), $E_{1.2}$ is the energy input rate of the air in the burners (W), E_2 is the energy output rate of the combustion gas in the burners (W), and E_R is the useful radiant power of the burners (W).

For the galvanising barrel:

The energy balance equation for the galvanising barrel is (See Fig. 4b):

$$0 = E_2 - E_3 - E_{Co} \quad (9)$$

where E_2 is the energy output rate of the combustion gas in the burners that enter in the galvanising barrel (W), E_3 is the energy output rate of the combustion gas in the galvanising barrel (W), and E_{Co} is the rate of energy production by convection (W).

For the system:

The energy balance equation for the system is (See Fig. 4b):

$$0 = (E_{1,1} + E_{1,2}) - E_3 - E_S \quad (10)$$

where $E_{1,1}$ is the energy input rate of the natural gas in the burners (W), $E_{1,2}$ is the energy input rate of the air in the burners (W), E_3 is the energy output rate of the combustion gas in the galvanising barrel (W), and E_S is the useful power rate of the system (W).

3.1.3. Energy efficiency

The equation that expresses the energy efficiency of the system is [34]:

$$\eta = \frac{E_{Usefull}}{E_{Input}} 100 \quad (11)$$

where η is the energy efficiency rate, $E_{Usefull}$ is the energy usefull rate (W), and E_{Input} is the energy input rate (W).

The energy efficiency equations corresponding to each component of the process are:

For the burners:

The energy efficiency equation for the burners is:

$$\eta_{burners} = \frac{E_R}{E_{1,1} + E_{1,2}} \cdot 100 \quad (12)$$

For the galvanising barrel:

The energy efficiency equation for the galvanising barrel is:

$$\eta_{barrel} = \frac{E_{Co}}{E_2} \cdot 100 \quad (13)$$

For the system:

The energy efficiency equation for the system is:

$$\eta_{system} = \frac{E_R + E_{Co}}{E_{1,1} + E_{1,2}} \cdot 100 \quad (14)$$

The Aspen HYSYS model discussed in the next section, Section 4, will provide the data necessary to perform these calculations.

3.2. Exergy analysis

Exergy analysis, which is also known as useful energy, is based on the first and second laws of thermodynamics and its general balance is express as follows [34]:

$$E_{Xdest} = \sum E_{Xin} - \sum E_{Xout} - \sum E_{Xloss} \quad (15)$$

where E_{Xdest} is the exergy destruction rate of the system (W), E_{Xin} is the exergy input rate (W), E_{Xout} is the exergy output rate (W), and E_{Xloss} is the exergy loss rate (W).

3.2.1. Fluids involved in the process

The exergy balance equations corresponding to each fluids involved in the process are:

For the natural gas:

The exergy rate of the natural gas can be calculated as follows [36]:

$$E_{XNG} = E_{XNG}^{ph} + E_{XNG}^{ch} \quad (16)$$

where E_{XNG} is the exergy rate of the natural gas (W), E_{XNG}^{ph} is the physical exergy rate of the natural gas (W), and E_{XNG}^{ch} is the chemical exergy rate of the natural gas (W). E_{XNG}^{ph} can be calculated as follows [36]:

$$E_{XNG}^{ph} = \sum_{i=1}^N n_{NGi} \cdot \left[C_{pNG}^h \cdot (T_{NG} - T_0) - T_0 \cdot C_{pNG}^s \cdot \ln \left(\frac{P_{NG}}{P_0} \right) + R \cdot T_0 \cdot \ln \left(\frac{P_{NG}}{P_0} \right) \right]_i \quad (17)$$

where n_{NGi} is the molar flux of natural gas (mol/s), C_{pNG}^h is the specific heat for enthalpies of natural gas (J/molK), T_{NG} is the temperature of the natural gas ($^{\circ}K$), T_0 is the dead state temperature which in our case

is the ambient temperature ($^{\circ}K$), C_{pNG}^s is the specific heat for entropies of natural gas (J/molK), P_{NG} is the natural gas pressure (kPa), P_0 is the dead state pressure which in our case is the ambient pressure (kPa), and R is the ideal gas constant which is 8.314472 (J/molK).

E_{XNG}^{ch} can be calculated as follows [34]:

$$E_{XNG}^{ch} = \sum_{i=1}^N \left[n_{NGi}^{C_xH_y} \cdot e_{exNG}^{C_xH_y} \right]_i \quad (18)$$

where $n_{NGi}^{C_xH_y}$ is the molar flux of each compound C_xH_y of the natural gas (mol/s), $e_{exNG}^{C_xH_y}$ is the specific chemical exergy rate of the natural gas (J/mol), and i is each of the C_xH_y components of natural gas.

The specific chemical exergy rate of each component of the natural gas with the form C_xH_y is [34]:

$$e_{exNG}^{C_xH_y} = Y_{f,C_xH_y} \cdot LHV_{C_xH_y} \quad (19)$$

$$Y_{f,C_xH_y} = 1.033 + 0.0169 \cdot \frac{y}{x} - \frac{0.0698}{y} \quad (20)$$

where Y_{f,C_xH_y} is the function of the degree of exergy of the compound C_xH_y , and $LHV_{C_xH_y}$ is the lower combustion power of each compound C_xH_y (J/mol).

For the air:

The exergy rate of the air can be calculated as follows [36]:

$$E_{XA} = E_{XA}^{ph} + E_{XA}^{ch} \quad (21)$$

where E_{XA} is the exergy rate of the air (W), E_{XA}^{ph} is the physical exergy rate of the air, and E_{XA}^{ch} is the chemical exergy rate of the air. E_{XA}^{ph} can be calculated as follows [36]:

$$E_{XA}^{ph} = \sum_{i=1}^N n_{Ai} \cdot \left[C_{pA}^h \cdot (T_A - T_0) - T_0 \cdot C_{pA}^s \cdot \ln \left(\frac{P_A}{P_0} \right) + R \cdot T_0 \cdot \ln \left(\frac{P_A}{P_0} \right) \right]_i \quad (22)$$

where n_{Ai} is the molar flux of air (mol/s), C_{pA}^h is the specific heat for enthalpies (J/molK), T_A is the temperature of the air ($^{\circ}K$), T_0 is the dead state temperature which in our case is the ambient temperature ($^{\circ}K$), C_{pA}^s is the specific heat for entropies (J/molK), P_A is the air pressure (kPa), P_0 is the dead state pressure which in our case is the ambient pressure (kPa), and R is the ideal gas constant which is 8.314472 (J/molK).

E_{XA}^{ch} can be calculated as follows [36]:

$$E_{XA}^{ch} = n_{TA} \cdot \sum_{i=1}^N \left[\chi_{Ai} \cdot \varepsilon_{0Ai} + R \cdot T_0 \cdot \chi_{Ai} \cdot \ln(\chi_{Ai}) \right]_i \quad (23)$$

where n_T is the molar flux of air (J/molK), χ_{Ai} is the mole fraction of each component of the air, ε_{0Ai} is the molar chemical exergy of each air component (J/mol), T_0 is the dead state temperature which in our case is the ambient temperature ($^{\circ}K$), and R is the ideal gas constant which is 8.314472 (J/molK).

For the flue gases:

In the same way, exergy rate is obtained from flue gases [36]:

$$E_{XFG} = E_{XFG}^{ph} + E_{XFG}^{ch} \quad (24)$$

where E_{XFG} is the exergy rate of the air (W), E_{XFG}^{ph} is the physical exergy rate of the air, and E_{XFG}^{ch} is the chemical exergy rate of the air. E_{XFG}^{ph} can be calculated as follows [36]:

$$E_{XFG}^{ph} = \sum_{i=1}^N n_{FGi} \cdot \left[C_{pFG}^h \cdot (T_{FG} - T_0) - T_0 \cdot C_{pFG}^s \cdot \ln \left(\frac{P_{FG}}{P_0} \right) + R \cdot T_0 \cdot \ln \left(\frac{P_{FG}}{P_0} \right) \right]_i \quad (25)$$

where n_{FGi} is the molar flux of flue gases (mol/s), C_{pFG}^h is the specific heat for enthalpies (J/molK), T_{FG} is the temperature of the flue gases ($^{\circ}K$), T_0 is the dead state temperature which in our case is the ambient temperature ($^{\circ}K$), C_{pFG}^s is the specific heat for entropies (J/molK), P_{FG} is the flue gases pressure (kPa), P_0 is the dead state pressure which in

our case is the ambient pressure (kPa), and R is the ideal gas constant which is 8.314472 (J/molK).

E_{XFG}^{ch} can be calculated as follows [36]:

$$E_{XFG}^{ch} = n_{TFG} \cdot \sum_{i=1}^N [\chi_{FGi} \cdot \varepsilon_{0FGi} + R \cdot T_0 \cdot \chi_{FGi} \cdot \ln(\chi_{FGi})]_i \quad (26)$$

where n_{TFG} is the molar flux of flue gases (J/molK), χ_{FGi} is the mole fraction of each component of the flue gases, ε_{0FGi} is the molar chemical exergy of each flue gases component (J/mol), T_0 is the dead state temperature which in our case is the ambient temperature ($^{\circ}$ K), and R is the ideal gas constant which is 8.314472 (J/molK).

3.2.2. Component of the process

The exergy balance equations corresponding to each component are:

For the burners:

The exergy balance equation for the burners is (See Fig. 3b):

$$0 = (E_{X1.1} + E_{X1.2}) - E_{X2} - E_{Xburnes,dest} \quad (27)$$

where $E_{X1.1}$ is the exergy input rate of the natural gas in the burners (W), $E_{X1.2}$ is the exergy input rate of the air in the burners (W), E_{X2} is the exergy output rate of the combustion gas in the burner (W), and $E_{Xburner,dest}$ is the exergy destroyed rate in the burners caused by entropy generation during combustion due to the entropy change in the reaction system and the heat lost during combustion in the immediate surroundings (furnace and galvanising barrel) (W).

For the galvanising barrel:

The exergy balance equation for the galvanising barrel is (See Fig. 3b):

$$0 = E_{X2} - E_{X3} - E_{Xbarrel,dest} \quad (28)$$

where E_{X2} is the exergy output rate of the combustion gas in the burners that enter in the galvanising barrel (W), E_{X3} is the exergy output rate of the combustion gas in the galvanising barrel (W), and $E_{Xbarrel,dest}$ is the exergy destroyed rate in the furnace due to heat transfer with the galvanising barril and the furnace walls (W).

For the system:

The exergy balance equation for the system is (See Fig. 3b):

$$0 = (E_{X1.1} + E_{X1.2}) - E_{X3} - E_{Xsystem,dest} \quad (29)$$

where $E_{X1.1}$ is the exergy input rate of the natural gas in the burner (W), $E_{X1.2}$ is the exergy input rate of the air in the burner (W), E_{X3} is the exergy output rate of the combustion gas in the galvanising barrel (W), and $E_{Xsystem,dest}$ is the exergy destruction rate of the system (W). This is the sum of the exergy destroyed in the burners due to entropy generation during combustion due to entropy change in the reaction system and heat lost during combustion in the immediate surroundings (furnace and galvanising barrel) and the exergy destroyed in the furnace due to heat transfer with the galvanising barrel and the furnace walls.

The expression of the exergy rate destroyed is [35]:

$$E_{Xdest} = T_0 \cdot S_{gen} \quad (30)$$

where T is the temperature ($^{\circ}$ K) and S is the generated entropy (J/ $^{\circ}$ K).

3.2.3. Exergy efficiency

The exergy analysis is being carried out on the basis of the combustion gases which, in our case, are interested in losing as much energy as possible in the form of heat to be transferred to the galvanising barrel to melt the zinc, therefore the efficiencies of the different elements will be given by the exergy destroyed in each one of them. The equation that expresses the exergy efficiency of the system is [34]:

$$\Psi = \frac{\sum E_{XUsefull}}{\sum E_{Xinput}} \cdot 100 \quad (31)$$

where Ψ is the exergy efficiency rate, $E_{XUsefull}$ is the exergy usefull rate (W), and E_{Xinput} is the exergy input rate (W).

The exergy efficiency equations corresponding to each component are:

For the burners:

The exergy efficiency equation for the burners is:

$$\Psi_{burners} = \frac{E_{Xburnes,dest}}{E_{X1.1} + E_{X1.2}} \cdot 100 \quad (32)$$

For the galvanising barrel:

The exergy efficiency equation for the burners is:

$$\Psi_{barrel} = \frac{E_{Xbarrel,dest}}{E_{X2}} \cdot 100 \quad (33)$$

For the system:

The total exergy efficiency equation for the system is:

$$\Psi = \frac{E_{Xsystem,dest}}{E_{X1.1} + E_{X1.2}} \cdot 100 \quad (34)$$

The Aspen HYSYS model discussed in the next section, Section 4, will provide the data necessary to perform these calculations.

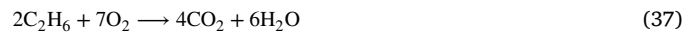
3.3. Sustainability analysis

The sustainability index (SI) provides information on the sustainability of the resources and is calculated based on the exergy efficiency as shown in the following expression [34]:

$$SI = \frac{1}{1 - \Psi} \quad (35)$$

3.4. CO₂ emissions

CO₂ emissions result from the combustion of natural gas in the burners. The combustion reaction can be expressed as:



The need for large amounts of energy in the production system and the extensive use of fossil fuels to obtain it generate large amounts of CO₂ emissions. Excessive CO₂ emissions are causing the acceleration of climate change and, therefore, ecological deterioration. One of the environmental problems that most concerns national governments is the emission of carbon dioxide (CO₂) in industrial processes [37]. Therefore, due to the urgent need to reduce CO₂ emissions, this indicator is essential. This indicator will be obtained with the Aspen HYSYS model studied in the next section, Section 4.

3.5. Fuel cost

In recent years, natural gas has been widely used in different industries: energy industry, chemical industry, etc. There are several reasons for this: (i) increased availability [38,39], (ii) less environmental damage [39,40], (iii) increasing economic competitiveness compared to other fossil fuel resources [39,40], (iv) low investment cost [39], (v) high energy conversion efficiency [41], and (vi) technological factors of gas installations [42]. However, as a fossil fuel, it has negative effects on the environment.

The quantification of the cost of the fuel used in the galvanising process is an important factor, as it helps to make decisions on the feasibility of the galvanising process. This indicator will be obtained with the Aspen HYSYS model studied in the next section, Section 4.

4. Material and method

The evaluation of the analyses set out in Section 3 in a process in which thermal energy generation predominates requires a detailed characterisation of the following aspects: the process itself, the thermal energy generation system, and the thermal losses of the flue gases. The proposed methodology is structured around these ideas. The methodology comprises the following steps:

- (i) Process analysis. The objective of this step is to analyse all relevant information in order to provide a global view to facilitate the modelling of the process. This step has already been discussed in Section 2.
- (ii) Experimental setup. To validate steps (iii) and (iv), the Aspen HYSYS model and the computational fluid dynamics (CFD) model, respectively, it is necessary to carry out measurements of operating parameters in the burners, in the galvanising barrel and in the furnace.
- (iii) Modelling of the flue gases using the Aspen HYSYS model. There are parameters that would require manual calculations that can be obtained in a more direct way through the Aspen HYSYS model. Such as the flue gas specific heat at the burner outlet, the flue gas molar flux at the burner outlet, etc. Determining these parameters is essential to be able to perform the next step, the modelling of the galvanising barrel using the computational fluid dynamics method. There are several software packages that can be used in this step. The Aspen HYSYS software has been used, as it has been used in similar works with excellent results [43–45].
- (iv) Modelling of the galvanising barrel using the computational fluid dynamics model. The modelling of the process by computational fluid dynamics (CFD), using parameters obtained with the Aspen HYSYS model and in the experimental setup, allows the complete process to be modelled. After a thorough review of the literature, SolidWorks software has been chosen, as it has been used in similar studies with excellent results [46,47].
- (v) Validation of the actual process. The CFD model obtained in step (iv) was validated using the operating conditions.

For the implementation of the CFD model it is necessary to know several input parameters to the model. These parameters are: (i) the energy provided, through the convection mechanism, by the combustion gases produced by the burners to the elements inside the furnace, such as the furnace walls and especially the galvanising barrel, which is the main element under study, and (ii) the radiant energy provided by the flame of the burners. In addition, for the validation of the model it is necessary to know temperature measurements at certain points of the process.

To obtain the energy of point (i), it is necessary to know the energy contained in all the gas streams involved in the process, such as: natural gas, air, and combustion gases inside and at the exit of the furnace. For this purpose, it is necessary to know for each of these gases the following parameters: (a) gas composition, (b) mass flow, (c) temperature, (d) pressure, (e) specific heat, and (f) density. Parameters (b), (c) and (d) are obtained by experimental measurements. And parameters (e) and (f) are obtained using the Aspen Hysys software.

To obtain the energy of point (ii), knowing the energies of the gas streams, equations (8) and (46) shall be applied to determine the radiation energy provided by the burner flame to the furnace elements.

Once the CFD model is implemented, experimental temperature measurements are used to validate the CFD model.

On the other hand, the Aspen HYSYS model also needs data obtained in the experimental setup, such as: (i) natural gas temperature at burner inlet, (ii) natural gas pressure at burner inlet, (iii) natural gas mass flow rate at burner inlet, (iv) air temperature at burner inlet, (v) air pressure at burner inlet, (vi) air mass flow rate at burner inlet, (vii) flue gas temperature at burner outlet, (viii) flue gas temperature

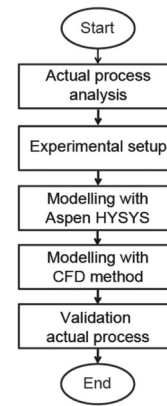


Fig. 5. Basic flowchart for modelling and validation.

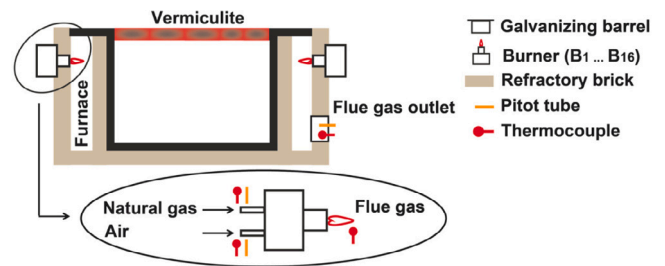


Fig. 6. Schematic drawing of the arrangement of the measuring devices.

Table 3
Characteristics of the measuring instruments used in the tests.

Parameter	Apparatus	Specifications
Absolute pressure	Testo 511 [48]	Measurement range: 300/1200 (hPa) Precision/resolution: 0.1 (hPa)
	Pitot tube	Measurement range: 0/1200 (hPa) Uncertainty: 1.7 (%)
Mass flow	Testo 350 [49]	Measurement range: 0/40 (m/s) Precision/resolution: 0.1 (m/s)
	Pitot tube	Measurement range: 0/40 (m/s) Uncertainty: 1.7 (%)
Temperature	Testo 440dp [50]	Measurement range: -200/1370 (°C) Precision/resolution: 0.1 (°C)
	Thermocouple	Measurement range: 0/1500 (°C) Uncertainty: 0.57 (%)

at furnace outlet, (ix) flue gas pressure at furnace outlet.

Fig. 5 shows the block diagram used in this methodology.

4.1. Experimental setup

To determine the Aspen HYSYS model and validate the computational fluid dynamics (CFD) model, measurements of operating parameters were carried out in the burners, in the galvanising barrel and in the furnace. These parameters are the following: (a) natural gas at burner inlet: temperature, pressure and mass flow; (b) air at the burner inlet: temperature, pressure, mass flow rate, and excess air ratio; (c) flue gas at the burner outlet: temperature; (d) flue gas at the furnace outlet: temperature, pressure, flow rate and CO load to be expelled in flue gases. The arrangement of the measuring devices used in the tests is shown schematically in Fig. 6.

4.1.1. Measuring instruments

The characteristics of the measuring instruments used in the tests are summarised in Table 3.

Table 4
Experimental results.

Parameter	Burner inlet	Burner outlet	Furnace outlet
Natural gas temperature (°K)	290.15		
Natural gas absolute pressure (kPa)	103.83		
Natural gas volumetric flow rate (m ³ /h)	1.90		
Air temperature (°K)	290.15		
Air absolute pressure (kPa)	103.83		
Air mass flow rate (m ³ /h)	40.33		
Flue gas temperature (°K)		873.15	605.25
Flue gas absolute pressure (kPa)			103.09

Table 5
Computed uncertainty of performance parameter.

Parameter	Parameters uncertainty (%)
Absolute pressure	1.7
Mass flow	1.7
Temperature	0.57

Given the difficulty of performing the tests during plant operation, the tests were conducted by a company specialised in this type of measurement. The company BUREAU VERITAS INSPECCION Y TESTING SLU [51] was in charge of carrying out the measurements of the parameters indicated above. All the equipment used is calibrated regularly.

4.1.2. Experimental results

The experimental results obtained are shown in Table 4.

4.1.3. Uncertainty analysis

Experimental results are affected by sources of error of different nature [52]. It is essential to consider these errors and the appropriate way is through an uncertainty analysis. When the parameter is measured directly, the measurement uncertainty is defined by the accuracy of the measuring device [52]. In contrast, when the parameter is calculated, the measurement uncertainty is determined based on the principle of the root-mean-square method [53]. In this case, the uncertainty determination involves: the measurement uncertainty of the parameter (e_R), the given function of the parameter (f), and the measurement uncertainties of the measured parameters (e_1, e_2, \dots, e_n). Using Eq. (40), the uncertainty can be evaluated:

$$e_R = \left[\left(\frac{\partial f}{\partial x_1} e_1 \right)^2 + \left(\frac{\partial f}{\partial x_2} e_2 \right)^2 + \dots + \left(\frac{\partial f}{\partial x_n} e_n \right)^2 \right]^{\frac{1}{2}} \quad (40)$$

Table 5 lists the uncertainties of the measured parameters.

The results obtained during experimentation can be considered to be of high accuracy if the uncertainty of each parameter is less than 2% [54] or 3% [52]. Therefore, the results obtained can be considered suitable for use in the remaining steps of the methodology.

4.2. Aspen HYSYS model

Aspen HYSYS [55] is a software that is characterised by its extensive library of component models and highly accurate property packages, thus, this software is a powerful process simulator. The connection of the diverse components is done by means of material and energy streams. Therefore, Aspen HYSYS can simulate simple and complex processes based on chemical/hydrocarbon fluids, both stationary and dynamic modes of operation [56,57].

For the simulation of the actual hot-dip galvanised steel wire process in Aspen HYSYS, the following assumptions are made:

- (i) The galvanising process is in steady state.
- (ii) The combustion of the natural gas is completed in the burner.
- (iii) The ratio of excess air in the burners adopted in the model is 1.87.

Table 6
Natural gas composition.

Component	CH ₄	C ₂ H ₆	C ₃ H ₈	C ₄ H ₁₀
% Volume	82	12.5	4	1.5

Table 7
Air composition.

Component	N ₂	O ₂	CO ₂	Ar
% Volume	78.04	20.99	0.03	0.94

- (iv) There are no flue gas leaks in the furnace.
- (v) The composition of the natural gas and air entering the burner are shown in Tables 6 and 7 [34,35].

- (vi) The inlet gases to each burner are natural gas and air, and are characterised by temperature, pressure and mass flow rate. These values obtained in the experimental setup are shown in Table 4.
- (vii) The reactions that take place in the burners are as follows [58]:



The limitations of the Aspen HYSYS model are directly related to the conditions assumed above:

- (i) The composition of air and natural gas must be as shown in Tables 6 and 7. Other studies have modelled natural gas as a mixture of pure methane [16], with very different results to those measured. Therefore, it is essential to properly model the composition of natural gas.
- (ii) If an excess air ratio other than 1.87 were used, the results would change significantly, as will be shown in the Results section.
- (iii) In reaction (41) taking place in the burners, 99.99% of the methane has to be consumed in the reaction. Using a different percentage affects the results.
- (iv) In the reaction (42) taking place in the burners 0.01% of the methane has been consumed. Using a different percentage affects the results.

As in similar studies [57], the Peng–Robinson fluid package was used to calculate the physicochemical properties, at different temperatures and pressures, of the following flows: natural gas, air and flue gas. Based on Fig. 4b, Fig. 7 shows the complete block flow diagram for the actual hot-dip galvanised steel wire system in Aspen HYSYS.

Each burner was simulated using a mixer and a conversion reactor (CRV-100.x in Fig. 7) in Aspen HYSYS. The natural gas stream, with the composition shown in Table 6, and the air stream, with the composition shown in Table 7, enter the mixer. The stream obtained from the mixture of natural gas and air is passed to the conversion reactor CRV-100, where the following reactions take place [58]: (41), (42), (43), (44), and (45).

The galvanising barrel is simulated by a cooler (E-100 in Fig. 7) in Aspen HYSYS. The flue gas streams from the 16 burners enter this cooler. A heat exchange takes place with the galvanising barrel and the properties of the flue gas leaving the furnace are obtained by entering the flue gas outlet pressure and temperature obtained in the experimental setup.

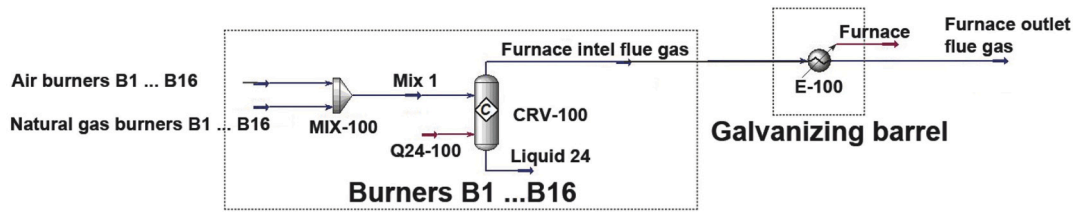


Fig. 7. Aspen HYSYS flowsheet diagram of the hot dip galvanizing process.

Table 8

The output parameters of the Aspen HYSYS model.

Parameter	Burners inlet	Burners outlet	Furnace outlet
Natural gas specific heat (kJ/kg°K)	2.060		
Natural gas density (kg/m ³)	0.845		
Natural gas volumetric flow rate (m ³ /h)	1.900		
Air specific heat (kJ/kg°K)	1.004		
Air density (kg/m ³)	1.247		
Air mass flow rate (m ³ /h)	40.325		
Flue gas specific heat (kJ/kg°K)		1.199	1.137
Flue gas density (kg/m ³)		0.406	0.581
Flue gas mass flow rate (m ³ /h)		2046.800	1428.688
Flue gas molar flux (kmol/h)		29.265	29.264
Flue gas mole fraction (CO ₂)		0.056	0.056
Flue gas mole fraction (N)		0.741	0.741
Flue gas mole fraction (O ₂)		0.093	0.093
Flue gas mole fraction (Ar)		0.009	0.009
Flue gas mole fraction (H ₂ O)		0.101	0.101
Flue gas mole fraction (CO)		0.000	0.000

The Aspen HYSYS model, in addition to the natural gas and air composition shown in Tables 6 and 7, respectively, requires the following input parameters obtained in the experimental setup (see Table 4): (i) natural gas temperature at burner inlet, (ii) natural gas pressure at burner inlet, (iii) natural gas mass flow rate at burner inlet, (iv) air temperature at burner inlet, (v) air pressure at burner inlet, (vi) air mass flow rate at burner inlet, (vii) flue gas temperature at burner outlet, (viii) flue gas temperature at furnace outlet, (ix) flue gas pressure at furnace outlet. Table 8 shows the parameters obtained with the Aspen HYSYS model.

One of the input parameters to the CFD model is the useful radiant power of each burner. This parameter can be determined using the results obtained with the Aspen HYSYS model. For this purpose, some of the results in Table 8 are used:

$$E_R = E_{NG} + E_A - E_{FG} \quad (46)$$

where E_R is the useful radiant power of each burner (W), E_{NG} is the energy rate of the natural gas (W), E_A is the energy rate of the air (W), and E_{FG} is the energy rate of the flue gases (W). E_{NG} , E_A and E_{FG} can be determined by Eqs. (5), (6), and (7) respectively.

Tables 4 and 8 show the parameters needed to apply equations (5), (6), and (7). The rate of energy input to each burner is 26.19 (kW) and the energy rate of the flue gases of each burner is 15.10 (kW). Therefore, the useful radiant power of each burner is 11.09 (kW).

4.3. Computational fluid dynamics modelling

The CFD solves the continuity, momentum and energy equations simultaneously in the galvanising barrel from experimental data and parameters obtained in the Aspen HYSYS model to determine the temperature distribution inside the galvanising barrel.

The equations for continuity, momentum and energy can be expressed as [59]:

The continuity equation:

$$\nabla \cdot (\rho \vec{v}) = 0 \quad (47)$$

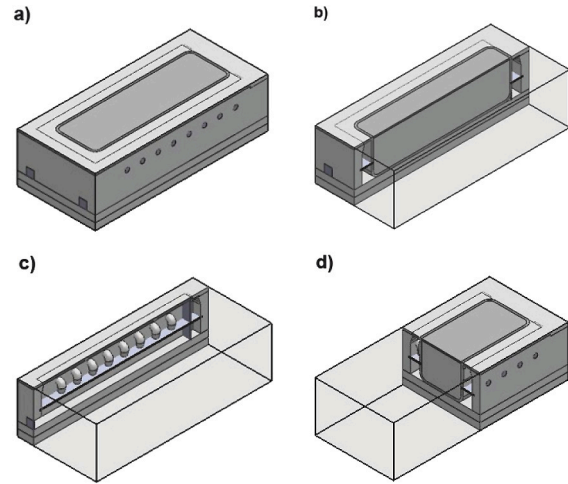


Fig. 8. Images of the SolidWorks design.

where ρ is the density, and \vec{v} is the fluid velocity in the control volume.

The momentum equation:

$$\rho \vec{v} + \nabla \vec{v} = \nabla p + \nabla \cdot \vec{\tau} + \rho \vec{g} \quad (48)$$

where p is the static pressure, ρ is the density, \vec{v} is the fluid velocity, and $\vec{\tau}$ is the Reynolds stress tensor.

The energy equation:

$$\nabla \cdot (\rho c_p \vec{v} T) = \nabla \cdot (k \nabla T) \quad (49)$$

where c_p is the specific heat, ρ is the density, T is the temperature and k is the thermal conductivity.

In Eqs. (47), (48) and (49) ∇ represents: $\nabla = \frac{\partial}{\partial x} + \frac{\partial}{\partial y} + \frac{\partial}{\partial z}$.

Solving Eqs. (47) and (49), which are strongly coupled and non-linear, is very complex, so a numerical approximation was used to solve them using commercial computational fluid dynamics software. Therefore, the governing equations were solved by the finite volume method using the solver package implicit in the software.

Firstly, the design of the galvanising barrel is carried out, and secondly, the simulation of the galvanising barrel is performed. The galvanising barrel has been designed in SolidWorks software [60] and simulated with SolidWorks Flow Simulation software [60]. Similar studies used SolidWorks software [61,62]. Fig. 8 shows several images of the SolidWorks design.

Fig. 8a shows the complete image of the design of the galvanising barrel. This image shows the gaps in the furnace through which the flue gases exit and the location of 8 burners. Fig. 8b shows a lengthwise section of the galvanising barrel where internal parts of the furnace and the galvanising barrel can be seen. Fig. 8c shows a lengthwise section of the galvanising barrel where 8 of the burners can be seen. Fig. 8d shows a cross-section of the galvanising barrel showing internal parts of the furnace and the galvanising barrel.

The numerical method used by the Solidworks Flow Simulation tool has an optimal behaviour for [60]: (i) incompressible flows, and

Table 9
Material properties.

Component	Material	Thermal conductivity (W/m ² K)	Density (kg/m ³)	Specific heat (J/kg ^o K)
Barrel	ARMCO iron	$-0.0675T + 97$ [60]	7874 [60]	$0.917T + 23.714$ [60]
Furnace	AISREF 125 refrac.	$0.0001T + 0.1027$ [66]	620 [66]	840 [66]
First floor	LITECAST 125 concr.	$0.0002T + 0.1354$ [66]	1310 [66]	880 [67]
Second floor	SIRCAST 125 concr.	0.8 [66]	1875 [66]	880 [67]
Zinc	Zinc	$-0.04T + 127$ [60]	7140 [60]	$0.171T + 514.5$ [60]
Vermiculite	Vermiculite	$0.000465T - 0.05272$ [68]	75 [68]	$2T + 443.7$ [68]

(ii) flows with Mach Numbers lower than 3.0. Some of the most important features of Solidworks Flow Simulation are [60]: (i) the good performance is based on the use of temporal approximations of the continuity and convection/diffusion equations (for momentum, temperature, etc.) together with an operator splitting technique; (ii) the heat radiation emitted and reflected by solid surfaces is considered to be diffuse. That is, they comply with Lambert's law, according to which the radiation intensity per unit area and per unit solid angle is the same in all directions; and (iii) it uses a discrete transfer model to simulate radiative heat transfer.

The boundary conditions are as follows:

- (i) The ambient temperature is 290.15 (°K).
- (ii) The atmospheric conditions with atmospheric pressure is 101.325 (kPa).
- (iii) The pressure at the flue gas outlet of the furnace is 103.09 (kPa).
- (iv) The initial temperature of the zinc is 724.15 (°K).
- (v) A rectangular prism was created around the galvanising barrel to decrease the simulation time, but without affecting the heat transfer mechanisms occurring in the galvanising barrel. The dimensions of the rectangular prism are: 4450 × 2000 × 1270.30 (mm).

The aspects taken into account with regard to the flow are as follows:

- (i) Turbulent flow conditions were considered during the simulation.
- (ii) Eqs. (47), (48) and (49) were solved using SolidWorks Flow Simulation software [60].
- (iii) The flow in the furnace was considered fully developed.
- (iv) A standard $k - \epsilon$ turbulence model was used to treat turbulence in the flow. That is, by means of the turbulent kinetic energy (k) and the turbulence dissipation rate (ϵ). This turbulent $k - \epsilon$ model is a common model used in similar studies [63–65].

The thermo-physical properties of the galvanising barrel, zinc and vermiculite, over the temperature range used in the study, are shown in Table 9 (in this table T is the temperature).

The limitations of the CFD model are as follows:

- (i) The thermo-physical properties of the components of the galvanising barrel, furnace, zinc and vermiculite, shown in Table 9. The use of other thermophysical properties will significantly affect the results.
- (ii) The dimensions of the galvanising barrel and furnace, as well as the height of the vermiculite, shown in Table 2. Changing any of these dimensions will also significantly affect the results.

In addition to the data shown in Table 9, other parameters obtained from the Aspen HYSYS model and the experimental setup are needed to perform the simulation. With respect to the Aspen HYSYS model, these values are as follows: useful radiant power of each burner outlet is 11.09 (kW), flue gas mass flow rate at the burner outlet is 51.91 (kg/h), and flue gas absolute pressure at the burner outlet is 103.83 (kPa). And with regard to experimental setup: flue gas temperature at the burner outlet is 873.15 (°K), and flue gas absolute pressure at the furnace outlet is 103.09 (kPa).

The computational mesh was created by SolidWorks Flow Simulation software [60]. The mesh is composed of hexahedral elements, automatically generated according to the Marching Voxel method [60]. The mesh used consists of two mesh models, a global mesh and a local mesh. The total number of cells used is 489019. Fig. 9 shows some meshes of the model. Fig. 9a shows a mesh in cross-section. Fig. 9b shows a mesh in the lengthwise section.

Fig. 10 shows some images of the temperature distribution in the galvanising barrel and in the furnace. Fig. 10a shows the temperature contours in the lengthwise section of the galvanising barrel half. Fig. 10b shows the temperature contours in a lengthwise section containing 8 of the burners. Fig. 10c shows the temperature contours in the galvanising barrel half. Fig. 10d shows the temperature contours in the cross-section in the flue gas outlet zone of the furnace.

4.4. Validation of the actual hot-dip galvanised steel wire process

To validate the model of the hot-dip galvanising steel wire process, the temperatures obtained with the CFD model were compared with the operating conditions of the actual hot-dip galvanising steel wire process. The hot-dip galvanising steel wire process was simulated under conditions identical to those of the experimental study, using input variables such as natural gas composition, temperature of natural gas at burner inlet, pressure of natural gas at burner inlet, mass flow of natural gas at burner inlet, etc.

Fig. 11 shows the reference system for locating the local temperature points ($LTPs$). Fig. 11a shows the general reference system. Fig. 11b shows the local temperature points in the lengthwise section of the galvanising barrel half. Local temperature points 1 to 9 are located inside the galvanising barrel. The local temperature points 24 to 26 are located inside the furnace. Fig. 11c shows the local temperature points in the lengthwise section furthest from the middle of the galvanising barrel. Local temperature points 10 to 19 are located inside the galvanising barrel. Local temperature point 10 is the location of the reference thermocouple. The local temperature points 27 to 29 are located inside the furnace. Fig. 11d shows the local temperature point 20 located at the furnace cross-section furthest away from the flue gas outlet of the actual hot-dip galvanised steel wire process. Fig. 11e shows the local temperature point 21 located in the furnace cross-section at the flue gas outlet of the actual hot-dip galvanised steel wire process. Fig. 11f shows the local temperature points 22 and 23 in the lengthwise section of the furnace.

The validation of the model was carried out from two points of view. Firstly, it was checked that the temperature values obtained in the model complied with the operating ranges of the hot-dip galvanising process provided by the company Moreda Riviere Trefilerías SA. For this purpose, 29 points were selected from the following elements of the process: inside the furnace, furnace walls and inside the galvanising tank. Secondly, the relative error of the following experimental measurements was determined: (i) Flue gas temperature burner outlet, (ii) Reference thermocouple temperature, and (iii) Flue gas temperature furnace outlet.

The operating conditions (1), (2), (3) must be used to validate the results obtained with those obtained experimentally. The reference system used to locate the point where the temperature is measured is

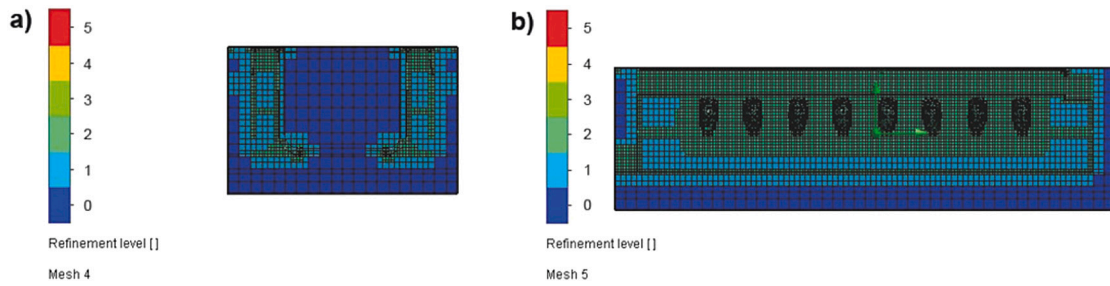


Fig. 9. Galvanising barrel mesh.

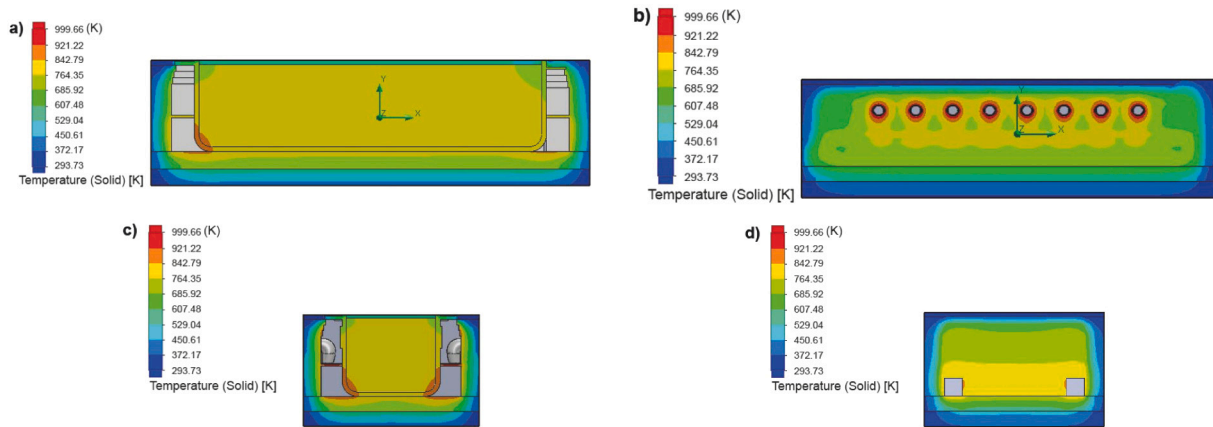


Fig. 10. Temperature distribution in the galvanising barrel and in the furnace from Solidworks Flow Simulation.

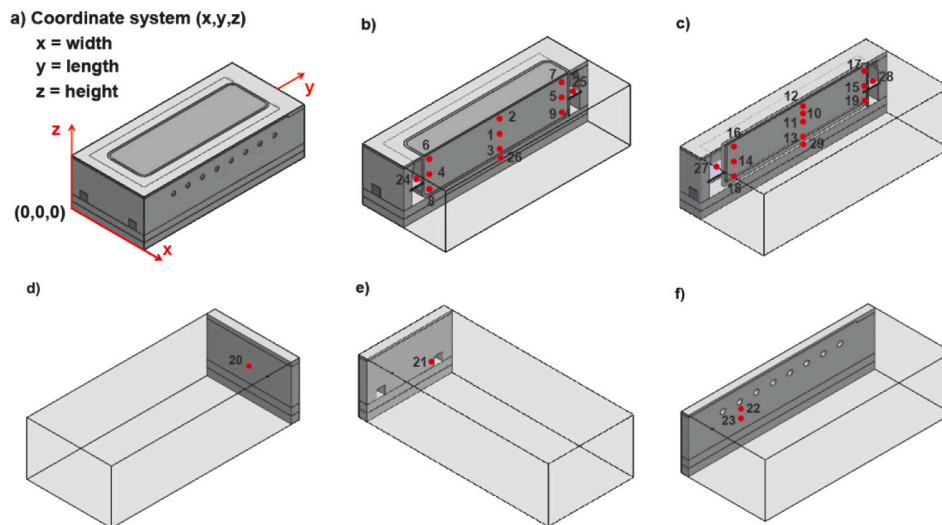


Fig. 11. Reference system for locating the local temperature points.

shown in Fig. 11. The local temperature points, according to Fig. 11, obtained with the CFD model are shown in Table 10 for the molten zinc and the furnace.

The results indicate that all the local temperature points analysed meet the operating conditions of the process.

The relative error (RE) shows the agreement between the experimental values and the values estimated by the model. Equation (50) is used to determine this indicator.

$$RE = \frac{T_p - T_a}{T_a} \cdot 100 \quad (50)$$

where T_p is the temperature of the predicted value and T_a is the temperature of the actual measured value. The results of equation

(50) can have negative and positive values, i.e. an underestimation or overestimation of the experimental values. If the result is close to 0, the model degree of accuracy is high.

Table 11 shows the reference thermocouple temperature measurement on 10 October 2024. The average value of this parameter is 747.82 (°K). The value of this parameter is very stable. Under normal operating conditions the temperature measurement made by the thermocouple can vary between ± 0.5 (°C) every 15 (min). If rare events occur, such as: a burner going out, increased production, etc., this variation can take values different from ± 0.5 (°C).

In addition, Table 4 shows the flue gas temperature at the burner outlet and the flue gas temperature at the furnace outlet. Table 12

Table 10
Results validation based on the operating condition.

LTP n°	LTP coord.	Component	Temp. (°K)	Condition verified (°K)
1	(1000, 2225, 805)	Molten zinc	804.69	$T_{Zn} \geq 692.68$ (1)
2	(1000, 2225, 1230)	Molten zinc	785.76	$T_{Zn} \geq 692.68$ (1)
3	(1000, 2225, 390)	Molten zinc	821.02	$T_{Zn} \geq 692.68$ (1)
4	(1000, 490, 805)	Molten zinc	798.66	$T_{Zn} \geq 692.68$ (1)
5	(1000, 3960, 805)	Molten zinc	785.11	$T_{Zn} \geq 692.68$ (1)
6	(1000, 490, 1230)	Molten zinc	726.97	$T_{Zn} \geq 692.68$ (1)
7	(1000, 3960, 1230)	Molten zinc	723.39	$T_{Zn} \geq 692.68$ (1)
8	(1000, 490, 390)	Molten zinc	850.84	$T_{Zn} \geq 692.68$ (1)
9	(1000, 3960, 390)	Molten zinc	832.89	$T_{Zn} \geq 692.68$ (1)
10	(503, 2225, 1155)	Molten zinc	752.12	$745.15 \leq T_{Ref} \leq 757.15$ (2)
11	(503, 2225, 805)	Molten zinc	798.50	$T_{Zn} \geq 692.68$ (1)
12	(503, 2255, 1230)	Molten zinc	741.89	$T_{Zn} \geq 692.68$ (1)
13	(503, 2255, 475)	Molten zinc	851.29	$T_{Zn} \geq 692.68$ (1)
14	(503, 490, 805)	Molten zinc	794.23	$T_{Zn} \geq 692.68$ (1)
15	(503, 3960, 805)	Molten zinc	779.55	$T_{Zn} \geq 692.68$ (1)
16	(503, 490, 1230)	Molten zinc	718.91	$T_{Zn} \geq 692.68$ (1)
17	(503, 3960, 1230)	Molten zinc	716.56	$T_{Zn} \geq 692.68$ (1)
18	(503, 490, 475)	Molten zinc	857.98	$T_{Zn} \geq 692.68$ (1)
19	(503, 3960, 475)	Molten zinc	849.64	$T_{Zn} \geq 692.68$ (1)
20	(1000, 4250, 750)	Furnace wall	827.01	$T_O \leq 893.15$ (3)
21	(1580, 200, 490)	Furnace wall	846.98	$T_O \leq 893.15$ (3)
22	(200, 1182, 875)	Furnace wall	890.66	$T_O \leq 893.15$ ((3))
23	(200, 1182, 805)	Furnace wall	793.64	$T_O \leq 893.15$ (3)
24	(1000, 320, 805)	Furnace	788.91	$T_O \leq 893.15$ (3)
25	(1000, 4080, 805)	Furnace	788.66	$T_O \leq 893.15$ (3)
26	(1000, 2225, 340)	Furnace	810.91	$T_O \leq 893.15$ (3)
27	(503, 320, 805)	Furnace	806.40	$T_O \leq 893.15$ (3)
28	(503, 4080, 805)	Furnace	811.24	$T_O \leq 893.15$ (3)
29	(503, 2225, 340)	Furnace	870.99	$T_O \leq 893.15$ (3)

Table 11
Reference thermocouple temperature measurement.

Date	Time	Reference thermocouple temperature (°K)
10/10/2024	11:47:33	748.4
10/10/2024	12:02:33	747.9
10/10/2024	12:17:33	747.4
10/10/2024	12:32:33	747.6

Table 12
Error study.

Parameter	Actual value (°K)	Estimated value		Error (%)
		LTP n°	Value (°K)	
Flue gas temperature burner outlet	873.15	28	811.24	-7.09
Reference thermocouple temperature	747.82	10	752.12	0.58
Flue gas temperature furnace outlet	605.25	21	846.98	39.94

shows the measured and estimated temperature values with the model, as well as the error made by the model in the estimation of these parameters.

Table 12 suggests the following conclusions:

- (i) The estimated value of the flue gas temperature at the burner outlet performs well considering the difficulty associated with flue gas modelling.
- (ii) The estimated value of the temperature measured by the thermocouple also performs well, with an error of less than 5 (°K).
- (iii) The estimated value of the flue gas temperature at the furnace outlet could not be determined with the model. The internal furnace wall temperature ($LTP\ n^\circ = 21$) has been measured with

Table 13
Energy analysis results of the fluids involved in the process.

Component	Fluids	Physical	Chemical	Energy rate (kW)
		energy rate (kW)	energy rate (kW)	
Burners inlet	Natural gas	4.261	349.652	353.914
Burners inlet	Air	65.122		65.122
Burners outlet	Flue gases	241.540		241.540
Furnace outlet	Flue gases	158.756		158.756

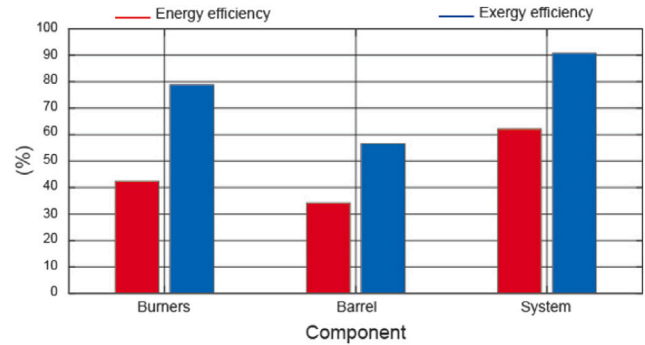


Fig. 12. Energy and exergy efficiencies of burners, galvanising barrel and system.

the model. However, due to the thickness of the furnace wall and the thermal properties of the furnace material, this value can also be considered acceptable.

The errors shown in Table 12 are much lower than those accepted in other studies [16]. These values suggest that the developed model is reliable.

5. Results and discussion

The performance of a hot-dip galvanising steel wire process, consisting of 16 burners, a galvanising barrel and a furnace, is investigated by means of energy, exergy and sustainability analysis. In addition, CO₂ emissions are also analysed.

5.1. Energy analysis

The results of the energy analysis of the fluids involved in the process are shown in Table 13.

According to the results shown in Table 13, galvanising 1 (kg) of wire requires 0.201 (kWh).

According to Table 13, the flue gases leaving the furnace contain a considerable amount of energy (158.756 (kW)), which leads to a decrease in the efficiency of the system. Therefore, other technologies could be used to recover the energy present in the flue gas.

Based on the results of the energy analysis (see Table 13), energy efficiencies can be calculated. For this purpose, Eqs. (12), (13) and (14) were used. The energy efficiencies of the burners, galvanising barrel, and system are shown in Fig. 12.

The efficiency of the burners is low because the air is not preheated before entering the burner.

The energy efficiency of the actual galvanising barrel is 55.34% [29], and the energy efficiency of the model is 62.11%, i.e. the model obtains an energy efficiency 6.77% higher. As the deviation is less than 10% [69], the model can be considered validated.

The energy efficiency of the system is 62.11%, therefore, this process is susceptible to the introduction of technologies that improve its results.

In Fig. 12 the energy efficiency is lower than the exergy efficiency, which is not common when assessing them. The reason for this is that the energy efficiency evaluates the energy of the gas streams in a more

Table 14
Exergy analysis results of the fluids involved in the process.

Component	Fluids	Physical exergy rate (kW)	Chemical exergy rate (kW)	Exergy rate (kW)
Burners inlet	Natural gas	0.0214	362.703	362.725
Burners inlet	Air	0.454	0.357	0.811
Burners outlet	Flue gases	69.546	7.176	76.722
Furnace outlet	Flue gases	26.121	7.176	33.298

generic way and does not take into account the quality and degradation of the energy in the process, so there is a part of heat contained in the energy carried by the flue gas stream that is not taken into account when calculating the efficiency.

In burners, the energy efficiency evaluates the heat provided by the flame through radiation as useful energy and takes the energy of the flue gas as losses, as the flue gas will be expelled from the system and the energy contained in it will be lost. However, as the exergy values the efficiency in the use of energy, it also takes into account that within the energy contained in the combustion gases, a percentage will correspond to heat expelled from the system and the rest will correspond to the work they can do, so the exergy efficiency is greater than the energy efficiency.

For the case of the barrel, the energy efficiency values the heat transmitted by convection of the flue gas stream from the time it leaves the burner until it leaves the furnace, but it does not take into account that part of the energy carried by these streams will also be heat absorbed by the system and that, therefore, the exergy, when evaluating this energy contained in the flue gases and dividing it as potential work of the flue gases and heat lost, will provide a higher efficiency than the energy efficiency.

In the case of the total system it is the same as for the burners and the barrel, the energy efficiency values the radiation energy contributed by the flame in the burners and the energy lost as convective heat from the flue gas stream from the time it leaves the burner until it leaves the furnace, but it does not take into account that part of the energy carried by these streams will be heat absorbed by the system.

5.2. Exergy analysis

The results of the exergy analysis of the fluids involved in the process are tabulated in Table 14.

Based on the results of the exergy analysis (see Table 14), exergy efficiencies can be calculated. For this purpose, Eqs. (32), (33) and (34) were used. The exergy efficiencies of the burners, galvanising barrel, and system are shown in Fig. 12.

5.3. Sustainability analysis

The sustainability index of the system, burners and galvanising barrel is 10.92, 4.74 and 2.30, respectively.

5.4. CO₂ emissions

According to the results obtained with the Aspen HYSYS model, the actual galvanisation process emits 72.61 (kg/h) of CO₂. This means that this process generates 636.06 (t) CO₂ per year. Therefore, galvanising 1 (kg) of wire emits 0.0348 (kg) of CO₂.

According to the results obtained with the Aspen HYSYS model, the flue gas temperature at the furnace exit is 605.24 (°K), and the flue gas flow rate at the furnace exit is 830.58 (kg/h). Therefore, the flue gas flow rate at the furnace outlet is 7,275.89 (t) per year. Specifically, annual CO₂ emissions are 636.06 (t). It can be concluded that the analysed process is very polluting.

5.5. Fuel cost

According to the technical data of the burners used in the galvanising process and the results obtained with the Aspen HYSYS model, the natural gas consumption is 25.67 (kg/h). This means that this process consumes 224.87 (t) of natural gas per year. Therefore, galvanising 1 (kg) of wire requires 0.0123 (kg) of natural gas.

The natural gas price of the Iberian Gas Market [70] was taken as the basis for the fuel cost study. The year 2023 was selected to frame the fuel cost study. Fig. 13 shows the average daily price of the Iberian Gas Market for the year 2023.

Using the daily prices shown in Fig. 13, the technical data of the burners, and the results obtained with the Aspen HYSYS model, the cost of the fuel used in the process studied can be determined. Fig. 14 shows the daily costs of the fuel used in the process.

It can be concluded that the analysed process has a high fuel cost.

5.6. Sensitivity analysis

One of the applications of this study is the ability to perform sensitivity analysis of parameters that affect energy and exergy efficiency. Once the hot-dip galvanising process is validated, there are several parameters that affect the energy and exergy efficiency. These parameters are [71]: (i) excess combustion air, and (ii) combustion air preheating. In these two scenarios, the CFD model has not been modified. In the section Other scenarios, possible modifications of the CFD model are proposed.

5.6.1. Excess combustion air

To improve the efficiency of the process it is necessary to use an excess air ratio that allows the complete combustion of the fuel, i.e. to use a minimum excess air ratio. According to Villaflor et al. [71] excess air increases the combustion gases and, consequently, the carbon dioxide emitted into the atmosphere, and consumes heat, increasing fuel consumption.

The excess air ratio used in the current hot-dip galvanising process, and therefore used in the Aspen HYSYS model, is 1.87. Two excess air ratios, 1.05 and 2.6, have been considered in this study. The results of these studies are shown in Fig. 15.

According to the simulations performed with the Aspen HYSYS model, for an excess air ratio of 1.05, which is lower than the excess ratio of the real process, the energy at the burner inlet is lower because the sensible heat supplied by the air is lower. However, by including less air in the combustion, the combustion gases decrease, increasing the energy efficiency in the burners from 42.36% to 63.28%, also increasing the exergy efficiency and, therefore, the useful energy. This also allows for less heat loss in the system, as the heat in the burners has been better utilised and less combustion gases have been generated, with the latter going from having an energy efficiency of 62.11% to 72%, also increasing, as before, its exergy efficiency and the useful heat utilised. In turn, these efficiencies translate into a temperature increase in the CFD model, but within the operating limits of the installation (see Table 15).

According to the simulations carried out with the Aspen HYSYS model, for an excess air ratio of 2.6, higher than the excess ratio of the real process, it can be observed that the energy efficiency of the burner decreases drastically, from 42.36% to 27.22%, also decreasing its exergy efficiency. Contrary to the previously analysed scenario, although the input energy increases as the sensible heat provided by the air increases, the quantity of combustion gases also increases and, therefore, so do the losses in the system, which decreases its energy efficiency from 62.11% to 52.07%, also decreasing its exergy efficiency and the useful heat used in the system. With respect to the temperatures of the model, there is a decrease in the same, not reaching the temperatures of the current model and, consequently, the operating conditions of the process (see Table 15).

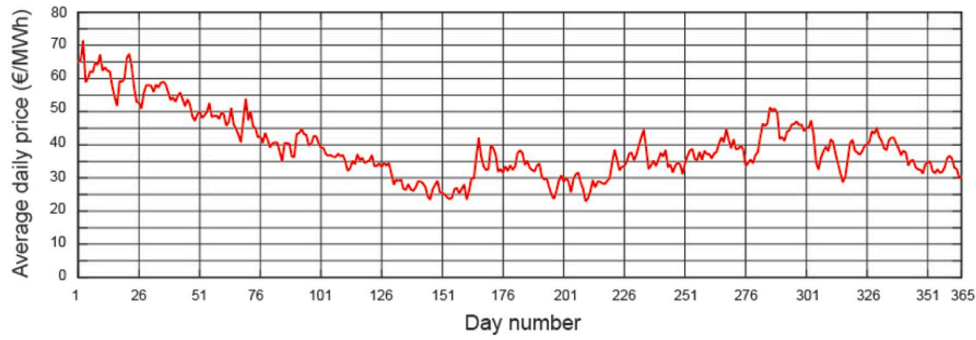


Fig. 13. Average daily price of the Iberian Gas Market (year 2023).

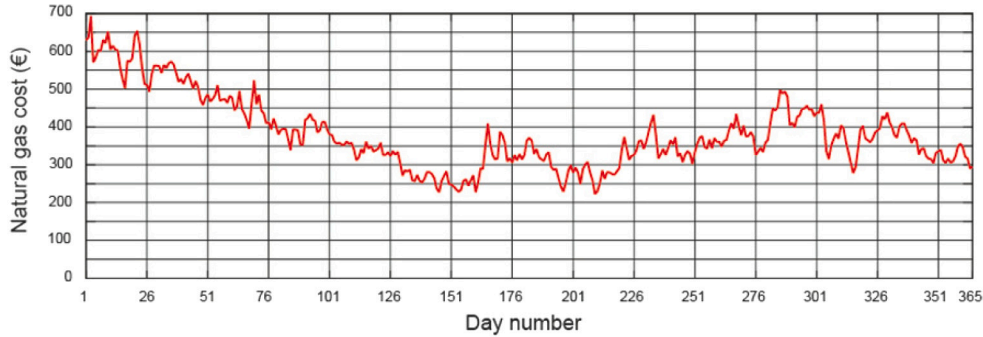


Fig. 14. Cost of the fuel (year 2023).

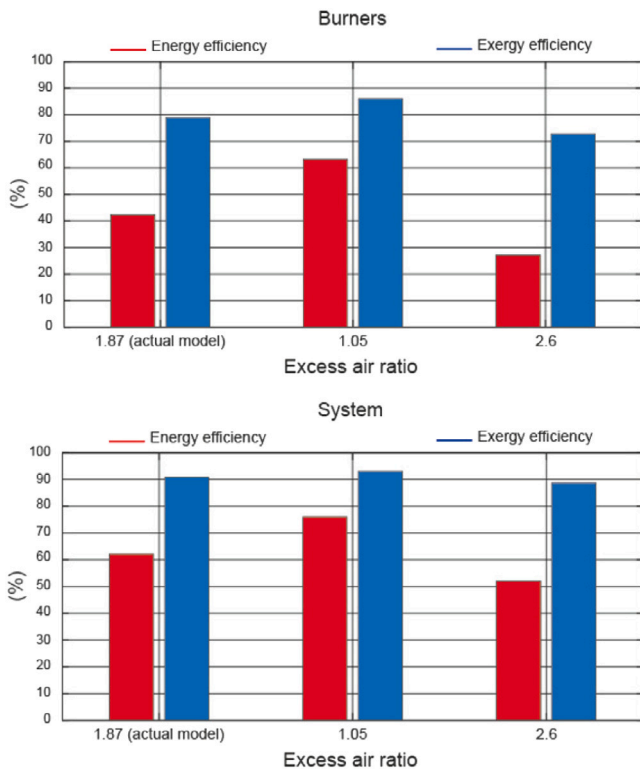


Fig. 15. Energy and exergy efficiencies of burners and system with excess combustion air.

Table 15 shows the temperature values estimated with the model with various excess air ratios.

Table 15 suggests the following conclusions:

- (i) The estimated value of the flue gas temperature at the burner outlet for the new excess air ratios studied complies with the operating condition. Obtaining similar values to those obtained with the current excess air ratio.
- (ii) The estimated value of the temperature by the thermocouple for the new excess air ratios studied does not adjust to the operating condition. Therefore, they would not meet this condition.
- (iii) As already mentioned, the estimated value of the flue gas temperature at the furnace exit could not be determined with the model. For the three excess air ratios studied, this temperature is similar.

It can be concluded that the incidence of the excess air ratio in the system could improve its efficiency if the excess air ratio were adapted to the minimum necessary for the complete combustion of the fuel. However, the current value of the excess air ratio is considered as the optimal option, since optimising the efficiency of the system would increase the temperatures in the galvanising vat above the current value of the process, which could have negative consequences on the coating of the wire [32], mechanical properties of the wire [72], etc.

5.6.2. Combustion air preheating

In this section the influence of combustion air preheating was analysed. A schematic of this procedure is shown in Fig. 16.

According to Jugjai and Rungsimuntuchart [73], air preheating at the burner inlet provides an improvement in system efficiency by decreasing fuel consumption and improving the combustion process.

According to the burner data sheet, the combustion air can be preheated up to 723.15 (°K), however, due to the temperature of the combustion gases at the furnace outlet, which is 605.24 (°K), they can preheat the combustion air up to a maximum of 601.15 (°K). This temperature allows the combustion gases not to reach the dew temperature after the heat exchange has taken place, thus avoiding the production of acid rain. For example, a single-pass cross-flow heat exchanger could be used, with the two flow fluids not mixed.

The temperature of the combustion air used in the current hot dip galvanising process, and therefore used in the Aspen HYSYS model, is

Table 15
Temperature values estimated with the model with various excess air ratios.

Parameter	LTP n°	Excess air ratio			Condition verified (°K)
		1.87	1.05	2.6	
		(actual)			
Flue gas temp. burner outlet	28	811.24	838.98	775.49	$T_O \leq 893.15$ (3)
Reference thermocouple temp.	10	752.12	784.47	723.46	$745.15 \leq T_{Ref} \leq 757.15$ (2)
Flue gas temp. furnace outlet	21	846.98	845.74	849.90	$T_O \leq 893.15$ (3)

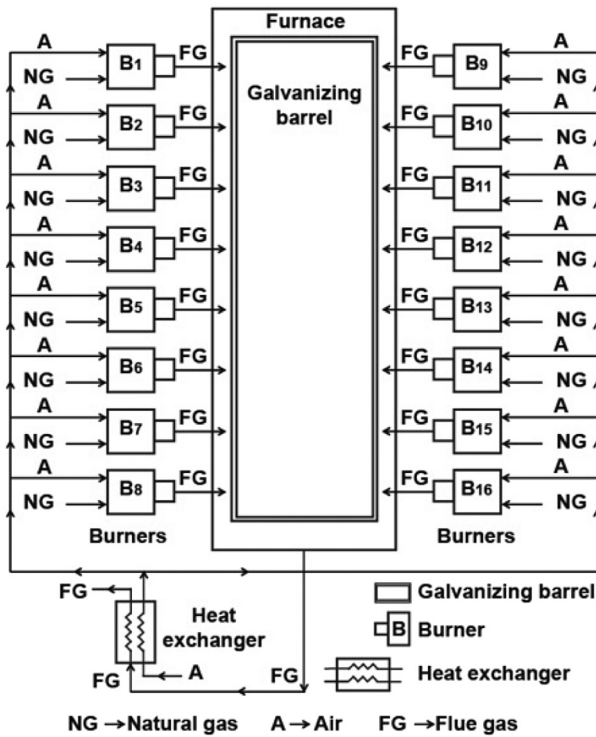


Fig. 16. Schematic of a combustion air preheating system.

290.15 (°K). Two combustion air preheating temperatures, 403.65 (°K) and 589.15 (°K), have been considered in this study. The results of these studies are shown in Fig. 17.

In the first scenario, preheating the combustion air to 403.65 (°K), natural gas consumption decreases by 7.80% without affecting the efficiency of the burners or the efficiency of the system. Obtaining very similar values to the current model, for example, the efficiency of the burners of the current model is 42.36% and with air preheating it is 42.79%. The same is true for the exergy efficiency, whose values are practically the same. For the system, in the current model, the energy efficiency is 62.11%, while in the model with preheated combustion air it is 62.38%.

In the second scenario, preheating of combustion air to 589.15 (°K), the decrease in natural gas consumption is 21.25%, the energy efficiency of the burners is slightly higher at 43.54% and the energy efficiency of the system is 62.84%. The same is true for the exergy efficiencies.

As for the temperatures obtained with the CFD models, for both scenarios with combustion air preheating, the temperatures are practically identical to those of the current model. Table 16 shows some of these results.

It can be concluded that the introduction of combustion air preheating techniques in the process would provide similar or slightly higher efficiencies [73], reducing the consumption of natural gas and making it possible to maintain adequate temperatures in the hot-dip

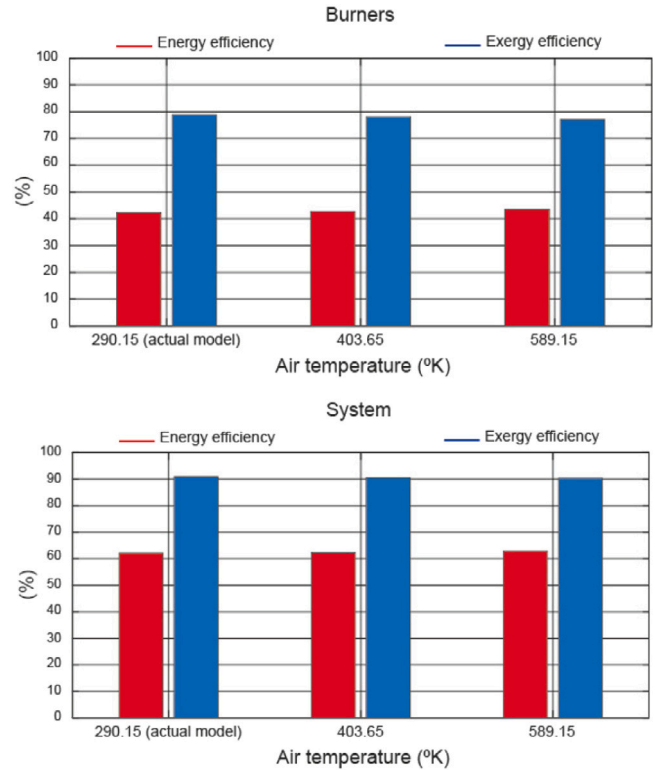


Fig. 17. Energy and exergy efficiencies of the burners and the system with combustion air preheating.

Table 16
Temperature values estimated with the model with air preheating at the burner inlet.

Parameter	LTP n°	Temp. of the air preheating			Condition verified (°K)
		290.15 (actual) (°K)	403.65 (°K)	589.15 (°K)	
Flue gas temp. burner outlet	28	811.24	811.52	811.38	$T_O \leq 893.15$ (3)
Reference thermocouple temp.	10	752.12	751.94	751.93	$745.15 \leq T_{Ref} \leq 757.15$ (2)
Flue gas temp. furnace outlet	21	846.98	846.66	847.01	$T_O \leq 893.15$ (3)

galvanising process.

5.6.3. Other scenarios

In the previous scenarios, the CFD model has not been modified. Two scenarios that would affect the CFD model are proposed here.

The first scenario would affect the modelling of the galvanising barrel. This new model would consist of a design in which the galvanising barrel is deeper and shorter, so that the wall for heat transfer is larger, reducing the attrition rate, but reducing the zinc surface area exposed to the atmosphere [16]. It is considered that decreasing the length of

the galvanising barrel would modify the way in which the steel wire is introduced into the molten zinc, making it more vertical, which could have an impact on its coating.

The second scenario, proposes the reduction of the space between the furnace wall and the surface of the galvanising barrel, which can provide a more uniform heat transfer in the system, although according to the literature, in this case the fuel consumption would have to be slightly increased to maintain the right temperature in the process [17]. It should be taken into account that the presence of radiant elbows that prevent the burner flame from directly hitting the galvanising barrel prevents a closer approach between the furnace wall and the barrel, besides the fact that it would not be optimal to increase fuel consumption, which would generate greater losses and greater pollution of the process by increasing the emissions of polluting gases.

6. Technologies to reduce CO₂ emissions and fuel costs in a hot-dip galvanised steel wire process

Due to the high amount of CO₂ emissions and fuel consumed by this process, it is necessary to propose strategies aimed at reducing fuel consumption (and consequently minimising operating cost), and reducing CO₂ emissions to mitigate environmental threats. Reducing the use of fossil fuels has become the energy strategy of most countries to achieve the goal of net-zero emissions [74]. The galvanising process is an energy-intensive industry, therefore it is necessary to improve its energy and environmental performance based on green technologies. Some of them are listed in this section. Based on the results of the above energy and exergy analyses, technologies can be proposed to reduce natural gas consumption, increase process efficiency and reduce CO₂ emissions. This section will propose technologies that can be implemented in the process under study to reduce CO₂ emissions and reduce fuel costs.

6.1. Use of new burner arrangements

The replacement of traditional natural gas burners with natural gas-fired ceramic immersion heaters would improve the efficiency of the process as the heat transfer would be directly to the molten zinc when immersed in it, avoiding heat transfer losses and improving the efficiency of the system. Tianjin Gongda Galvanising Equipment Co., Ltd [75] markets this type of burner. This work could be used as a starting point for future research on the use of this type of burners in a hot-dip galvanising process. With the use of this type of burner, savings in natural gas consumption are expected by improving the heat transfer mechanism of the process.

6.2. Hydrogen-enriched natural gas

Hydrogen is becoming a key enabler for sustainable development, as it is a clean, efficient, renewable and low-carbon energy source. Several studies have focused on the blending of hydrogen and natural gas [76,77]. This blend has several advantages, such as [76]: (i) it could utilise the existing natural gas transportation network, facilitating the long-distance and large-scale transportation of green hydrogen, (ii) hydrogen-enriched natural gas can reduce natural gas consumption, carbon dioxide and pollutant emissions, (iii) the combustion gases from this blend have a higher water vapour content and a higher latent heat of condensation. Hydrogen-enriched natural gas can be used in natural gas boilers [78], gas internal combustion engines and gas turbines [79].

As the composition of the hydrogen-natural gas mixture is different from the natural gas mixture used in this work, a new Aspen HYSYS model is necessary. The same is true for the flue gas composition of the mixture, which will change because the flue gas of the hydrogen-natural gas mixture has a higher water vapour content than that of the pure natural gas combustion. Therefore, this work can be used as a starting point for future research on the use of the hydrogen/natural gas

mixture in the hot-dip galvanising process. Deymi et al. [80] studied the effect of hydrogen mixing on different components of natural gas and concluded that if the hydrogen concentration is between 1 to 10% there is no need to upgrade the original equipment. Cakir et al. [77] analysed the adaptation of hydrogen-doped pipelines, and concluded that when the hydrogen mixing ratio is less than 20 vol%, the existing pipeline network will not be affected. The natural gas savings will depend on the percentage of hydrogen in the enriched natural gas.

6.3. Cogeneration systems

The Directive on energy efficiency, adopted in 2012 (Directive 2012/27/EU [81]), was updated in 2018 and 2023, promoted industrial processes of combined heat and power generation (cogeneration), as most industrial processes have simultaneous demands for electricity and heat. The integration of cogeneration systems in production processes can offer several advantages: [82]: (i) a decrease in primary energy consumption in combined heat and power generation compared to stand-alone heat and power generation; (ii) a reduction in greenhouse gas emissions; and (iii) the possibility of improving the manufacturing process by generating electricity and heat simultaneously.

The implementation of a cogeneration system in a production process has high investment costs. However, the adoption of cogeneration systems is financially supported. A good example is the EU [83], which promoted several legislative provisions to establish a harmonised framework for cogeneration systems.

Cogeneration technologies have received special attention worldwide due to their potential for energy conservation and greenhouse gas reduction [84]. Cogeneration recovers heat lost in one system to operate other systems. A typical cogeneration system is composed of an engine (equipped with an electric generator) and a heat distribution system to transfer heat to the users. For example, the flue gases from a burner enter the heat recovery generator, and the heat from these gases generates electrical energy. Cogeneration systems normally use natural gas as fuel for engines or turbines to produce electricity and heat at the same time [35].

There are several technological options for a cogeneration system. For example, gas turbine [85], diesel engine [86], geothermal turbine [87], steam turbine [88], micro-turbines [89], and Stirling engine [86]. Stirling engine is increasing their popularity, mainly in the mini and micro scale [90]. This is due to its multi-fuel capability, low fuel consumption, high efficiency, clean combustion, low noisy levels and low temperature operation [91]. The thermodynamic cycle in which these engines operate is the Stirling cycle, whose efficiency is theoretically equivalent to that of the Carnot cycle [92]. This is a highly idealised thermodynamic cycle, which includes two isothermal and two isochoric processes and is thermodynamically reversible. An example of the use of these engines is a sewage treatment plant in Sachsen Niederfrohna [90], which uses sewage gas as fuel for heat production in a Stirling engine. In operation, it has 125 (kW) of total rated thermal input delivered in the form of gas and it obtains 35.6 (kW) of electrical power, getting a 70% of heat generation efficiency. Therefore, Stirling engine systems continue to be the best choice in the mini and micro scale due to their high overall efficiency, favourable thermal to electricity power ratios and lower emissions than internal combustion engine systems [93].

There are many examples of the implementation of cogeneration systems in industrial processes, for example: paper industry, ceramic industry, textile industry, sugarcane industry, etc. This work could be used as a starting point for future research on the implementation of a cogeneration system in a hot-dip galvanising process.

6.4. Solar thermal energy

The integration of solar thermal technologies in an industrial process has to guarantee the necessary thermal energy and temperature

level required by the industrial process. The operating temperature of the industrial process selects the solar thermal technology to be used. Vannoni et al. [94] classified European industries requiring thermal energy according to their operating temperature as follows: 30% of industrial processes require thermal energy below 100 (°C), 27% operate between 100 and 400 (°C), and the remaining 43% require thermal energy above 400 (°C). Solar thermal technologies that can be used to generate thermal energy in industrial processes can be classified as solar air collectors, solar water systems and solar concentrators. Each of these technologies will be discussed below:

(i) Solar air collectors.

Solar air collectors were mainly implemented in the food industry. They operate at temperatures between 40 and 100 (°C) [95]. They are used in food drying and can replace gas or oil drying. Different designs are available [96]. Solar drying technologies can be grouped into (a) direct and indirect solar dryers, and (b) active and passive solar dryers. In direct solar dryers the solar irradiance is directly incident on the food, and in indirect solar dryers the loss of food quality due to the action of *UV* rays is avoided. Air circulation driven by natural convection and wind pressure is used in passive systems. These systems do not consume electrical energy. Air circulation in active systems is by means of fans, and therefore, they consume electrical energy. The drying time is shorter in active systems.

(ii) Solar water systems.

Solar water systems are classified as flat plate collectors or evacuated tube collectors, although they are mainly used in the building sector, they can also be implemented in industrial processes to provide a heat demand of up to 125 (°C).

(iii) Solar concentrators.

Solar concentrators include parabolic dish collectors (340 to 1200 (°C) [97]), compound parabolic collectors (340 to 560 (°C) [97]), linear Fresnel collectors (340 to 540 (°C) [97]), and solar tower (400 to 3000 (°C) [97]). Some examples of the application of these technologies are: automobile industry, mineral processing industry, dairy industry, etc.

With some changes to the galvanising barrel, this work could be used as a starting point for future research on the implementation of solar thermal energy in a hot-dip galvanising process.

Fossil fuel savings are guaranteed by using solar energy, which is free and inexhaustible. Moreover, as it is clean, it also guarantees a reduction in CO₂ emissions.

6.5. PV systems

Decarbonisation of the hot-dip galvanising process could be achieved by switching from fossil fuel, natural gas, to electric power. This electrical energy could be obtained from a photovoltaic system installed in the industry itself. To do this, a new galvanising barrel would have to be designed and the operating temperatures of the process could be obtained by means of resistors submerged in the molten zinc. This type of resistors is still underdeveloped and few companies are marketing them. The company Tianjin Gongda Galvanising Equipment Co., Ltd [75] markets this type of resistors. The company offers several novel solutions including ceramic electric immersion heaters for hot-dip galvanising processes and alloy electric immersion heaters for hot-dip galvanising processes. Each of these resistors uses different compounds in the sleeves to protect the resistor from attack by the zinc bath in which they are immersed. With some changes to the galvanising barrel, this work could be used as a starting point for future research on the implementation of solar thermal energy in a hot-dip galvanising process.

Fossil fuel savings are guaranteed by using solar energy, which is free and inexhaustible. Moreover, as it is clean, it also guarantees a reduction in CO₂ emissions.

7. Conclusions

This work investigates an energy, exergy, sustainability, environmental emissions and fuel cost analysis of a hot-dip galvanised steel wire process as a starting point for the inclusion of clean technologies in this process. Actual hot-dip galvanised steel wire process belonging to the company Moreda Riviere Trefilerías S.A. (Spain) is used as the basis for this study. In order to carry out the thermodynamic analysis of the process, it is necessary to know several parameters, for which a methodology is proposed. This methodology comprises the following steps: a process analysis, an experimental setup, a modelling of the flue gases using the Aspen HYSYS model, a modelling of the galvanising barrel using the computational fluid dynamics model, and a validation of the process. According to the experimental analysis, the proposed models (the Aspen HYSYS model and the computational fluid dynamics model) were validated, as they meet the operating conditions of the process. The following conclusions are drawn:

- (i) The energy efficiency of the system, burners and galvanising barrel is 62.11%, 42.36% and 34.27%, respectively.
- (ii) The exergy efficiency of the system, burners and galvanising barrel is 90.84%, 78.90% and 56.60%, respectively.
- (iii) The sustainability index of the system, burners and galvanising barrel is 10.92, 4.74 and 2.30, respectively.
- (iv) The galvanising process emits 72.61 (kg/h) CO₂, i.e. 636.06 (t) CO₂ per year. Therefore, galvanising 1 (kg) of wire in the actual process emits 0.0348 (kg) of CO₂.
- (v) The natural gas consumption is 25.67 (kg/h), i.e. 224.87 (t) of natural gas per year. Therefore, galvanising 1 (kg) of wire requires 0.0123 (kg) of natural gas.

The above results allow the study of the hot-dip galvanising process to be extended. As future work, the aim is to study the possible new improvements and technologies presented in the previous section, such as: (i) the insertion of cogeneration modules in the model, assessing the optimum way of incorporating them, increasing the efficiency of the installation as much as possible, (ii) the use of hydrogen-enriched natural gas. As the composition of the hydrogen-natural gas mixture is different from the natural gas mixture used in this work, a new Aspen HYSYS model is needed, (iii) the use of resistors, developed by the company Tianjin Gongda Galvanising Equipment Co., Ltd, powered by a photovoltaic system, so that the study can check whether the resistors can be incorporated into a new design of the galvanising barrel, making it possible to analyse the efficiency and sustainability of the process, (iv) the use of solar thermal energy to obtain the heat needed to melt the zinc, designing a new galvanising barrel that makes it possible to analyse the efficiency and sustainability of the process, and (v) the joint use of these systems.

CRedit authorship contribution statement

T. Álvarez-Álvarez: Writing – review & editing, Writing – original draft, Software, Methodology, Conceptualization. **A. Barbón:** Methodology, Conceptualization. **L. Bayón:** Methodology, Conceptualization. **C.A. Silva:** Writing – review & editing, Software, Methodology.

Declaration of competing interest

The authors declare that they have no known competing financial interests or personal relationships that could have appeared to influence the work reported in this paper.

Acknowledgments

We wish to thank Moreda Riviere Trefilerías S.A. [29] for his contribution in this paper.

Data availability

Data will be made available on request.

References

- [1] Shibli S, Meena B, Remya R. A review on recent approaches in the field of hot dip zinc galvanizing process. *Surf Coatings Technol* 2015;262:210–5.
- [2] World steel association. 2024, <https://worldsteel.org/es/media/press-releases/2024/december-2023-crude-steel-production-and-2023-global-totals/>.
- [3] American galvanizers association: Hot-dip galvanizing for corrosion protection a specifier's guide. 2012, <https://galvanizeit.org/inspection-course/galvanizing-process/time-to-first-maintenance1>.
- [4] NACE international. 2024, <http://impact.nace.org/economic-impact.aspx>.
- [5] Liu Y, Gao H, Wang H, Tao X, Zhou W. Study on the corrosion behavior of hot-dip galvanized steel in simulated industrial atmospheric environments. *Int J Electrochem Sci* 2024;19:100445.
- [6] Barchart. <https://www.barchart.com/story/news/18754551/galvanized-steel-market-trends-2023-2030-future-developments-and-insights>.
- [7] Arguillarena A, Margallo M, Urriaga A. Carbon footprint of the hot-dip galvanisation process using a life cycle assessment approach. *Clean Eng Technol* 2021;2:100041.
- [8] UNE-EN ISO 1461. Hot dip galvanizing coatings on fabricated iron and steel articles - specifications and test methods. 2009.
- [9] Woolley T. Galvanizing and sustainable construction. *European General Galvanizers Association*; 2008, p. 1–42.
- [10] Åhman M, Nilsson LJ, Johansson B. Global climate policy and deep decarbonization of energy-intensive industries. *Clim Policy* 2016;17(5):634–49.
- [11] EU European Commission. Directive 2003/87/EC, establishing a scheme for greenhouse gas emission allowance trading within the community and amending council. 2003, <https://eur-lex.europa.eu/legal-content/EN/TXT/PDF/?uri=CELEX:32003L0087&from=EN>.
- [12] EU European Commission. Directive 2009/29/EC, As to improve and extend the greenhouse gas emission allowance trading scheme of the community. 2009, <https://eur-lex.europa.eu/LexUriServ/LexUriServ.do?uri=OJ:L:2009:140:FULL:EN:PDF>.
- [13] EU European Commission. Directive 2012/27/EU, On energy efficiency. 2012, <https://eur-lex.europa.eu/LexUriServ/LexUriServ.do?uri=OJ:L:2012:315:FULL:EN:PDF>.
- [14] EU European Commission. A Roadmap for moving to a competitive low carbon economy in 2050. 2011, <https://eur-lex.europa.eu/LexUriServ/LexUriServ.do?uri=COM:2011:0112:FIN:en:PDF>.
- [15] Sanguanmoo R, Nisaratanaporn E, Boonyongmaneerat Y. Hot-dip galvanization with pulse-electrodeposited nickel pre-coatings. *Corros Sci* 2011;53:122–6.
- [16] Blakey SG, Beck SBM. The effect of combined radiation and convection on hot dip galvanizing kettle wear. *Appl Therm Eng* 2004;24:1301–19.
- [17] Manoj P, Sonal P, Amit P. Thermal analysis of the molten lead kettle failure at the galvanizing plant and development of novel design using CFD techniques. *Int J Innov Res Sci Eng Technol* 2015;4:1351–60.
- [18] Dewa M, Dzwaïro B, Nleya B. Evaluation of electrical energy consumption by a hot-dip galvanising plant. In: *Proceedings of the 27th annual southern african institute for industrial engineering conference*. 2016.
- [19] Szymczyk J, Kluczek A. Increasing the energy efficiency of a hot-dip galvanizing plant and reducing its environmental impact. *J Power Technol* 2017;97:349–58.
- [20] Gu Z, Liu Z, Yang S, Xie N, Ma K. Exergy and environmental footprint analysis for a green ammonia production process. *J Clean Prod* 2024;455:142357.
- [21] Yao Y, He J-Y, Chen Q, Li T, Li B, X-L. Wei. Analysis of energy, exergy and CO₂ emissions in a fiberglass furnace with oxy-fuel combustion. *Fuel* 2023;348:128484.
- [22] Sun J, Na H, Yan T, Qiu Z, Yuan Y, He J, et al. A comprehensive assessment on material, exergy and emission networks for the integrated iron and steel industry. *Energy* 2021;235:121429.
- [23] Parvez M, Ahamad T, Lal S, Khan O, Khalid F, Yahya Z. Energy, exergy, economic, and environmental assessment of a trigeneration system for combined power, cooling, and water desalination system driven by solar energy. *Int J Thermofluids* 2024;22:100694.
- [24] Caglayan H, Caliskan H. Assessment of a cogeneration system for ceramic industry by using various exergy based economic approaches. *Renew Sustain Energy Rev* 2022;167:112728.
- [25] Khanmohammadi S, Saadat-Targhi M, Nabati A. Energy and exergy analyses of a new integrated system for textile factory using geothermal energy source. *Energy* 2022;257:124696.
- [26] Tagnamas Z, Lamsyehe H, Moussaoui H, Bahammou Y, Kouhila M, Ildlimam A, et al. Energy and exergy analyses of carob pulp drying system based on a solar collector. *Renew Energy* 2021;163:495–503.
- [27] Bühler F, Nguyen T-V, Kjær Jensen J, Müller Holm F, Elmegaard B. Energy, exergy and advanced exergy analysis of a milk processing factory. *Energy* 2018;162:576–92.
- [28] Mol da Silva G, Guimarães Ferreira A, Morouço Coutinho R, Brasil Maia C. Energy and exergy analysis of the drying of corn grains. *Renew Energy* 2021;163:1942–50.
- [29] Moreda Riviere Trefilerías S.A. <https://moreda.com/>.
- [30] UNE-EN 1179. Zinc and zinc alloys. Primary zinc. 2004.
- [31] Kromschroeder. <https://www.kromschroeder.es/productos-kromschroeder>.
- [32] Bicao P, Jianhua W, Xuping S, Zhi L, Fucheng Y. Effects of zinc bath temperature on the coatings of hot-dip galvanizing. *Surf Coat Technol* 2008;202:1785–8.
- [33] Kartal F, Özveren U. A comparative study for biomass gasification in bubbling bed gasifier using Aspen HYSYS. *Bioresour Technol Rep* 2021;13:100615.
- [34] Caglayan H, Caliskan H. Energy, exergy and sustainability assessments of a cogeneration system for ceramic industry. *Appl Therm Eng* 2018;136:504–15.
- [35] Gürtürk M, Oztop HF. Exergy analysis of a circulating fluidized bed boiler cogeneration power plant. *Energy Convers Manage* 2016;120:346–57.
- [36] Kotas TJ. *The exergy method of thermal plant analysis*. London, UK: Butterworth Publishers; 1985.
- [37] Bouckaert S, Pales AF, McGlade C, et al. Net zero by 2050: a roadmap for the global energy sector. *International Energy Agency (IEA)*; 2021, <https://www.iea.org/reports/net-zero-by-2050>.
- [38] Mittakola RT, Ciaï P, Zhou C. Short-to-medium range forecast of natural gas use in the United States residential buildings. *J Clean Prod* 2024;437:140687.
- [39] Babaei F, Bozorgmehry Boozarjomehry R, Khairkhan Ravandi Z, Pishvaie SMR. A techno-economic analysis framework for power system-aware co-expansion planning of integrated gas transmission networks and chemical industries toward a more sustainable management of multi-energy systems. *Sustain Energy, Grids Networks* 2022;32:100893.
- [40] Al-Hamed K, Dincer I. Natural gas as a transitional solution for railway powering systems: Environmental and economic assessment of a fuel cell based powering system. *J Nat Gas Sci Eng* 2020;80:103347.
- [41] Balli O, Caliskan H. Various thermoeconomic assessments of a heat and power system with a micro gas turbine engine used for industry. *Energy Convers Manage* 2022;252:114984.
- [42] Pambour KA, Erdener BC, Bolado-Lavin R, Dijkema GP. SAInt-A novel quasi-dynamic model for assessing security of supply in coupled gas and electricity transmission networks. *Appl Energy* 2017;203:829–57.
- [43] Worsham EK, Terry SD. Static and dynamic modeling of steam integration for a NuScale small modular reactor and pulp and paper mill coupling for carbon-neutral manufacturing. *Appl Energy* 2022;325:119613.
- [44] Mehrpooa M, Tosang E, Dadak A. Investigation of a combined cycle power plant coupled with a parabolic trough solar field and high temperature energy storage system. *Energy Convers Manage* 2018;171:1662–74.
- [45] Tian C, Su C, Yang C, Wei X, Pang P, Xu J. Exergetic and economic evaluation of a novel integrated system for cogeneration of power and freshwater using waste heat recovery of natural gas combined cycle. *Energy* 2023;264:126227.
- [46] Regalado-Rodríguez N, Militello C. Comparative study of the effects of increasing heat transfer area within compression and expansion chambers in combination with modified pistons in stirling engines. A simulation approach based on CFD and a numerical thermodynamic model. *Energy Convers Manage* 2022;268:115930.
- [47] Barbón A, López-Smeets C, Bayón L, Pardellas A. Wind effects on heat loss from a receiver with longitudinal tilt angle of small-scale linear fresnel reflectors for urban applications. *Renew Energy* 2020;162:2166–81.
- [48] TESTO. Testo 511. <https://static-int.testo.com/media/fc/5b/31861cf0dae/testo-511-Instruction-manual.pdf>.
- [49] TESTO. Testo 350. <https://static-int.testo.com/media/d1/56/d4836ea87dd7/testo-350-Instruction-Manual.pdf>.
- [50] TESTO. Testo 440dp. <https://static-int.testo.com/media/51/05/0c73c53b9b04/testo-440-Instruction-Manual.pdf>.
- [51] BUREAU VERITAS INSPECCION. <https://www.bureauveritas.es/>.
- [52] Li M, Zhang Q, Li G, Shao S. Experimental investigation on performance and heat release analysis of a pilot ignited direct injection natural gas engine. *Energy* 2015;90:1251–60.
- [53] Rahman MM, Hamada KI, Aziz ARA. Characterization of the timeaveraged overall heat transfer in a direct-injection hydrogen-fueled engine. *Int J Hydrog Energy* 2013;38:4816–30.
- [54] Al-Waeli AHA, Chaichan MT, Sopian K, Kazem HA, Mahood HB, Khadom AA. Modeling and experimental validation of a PVT system using nanofluid coolant and nano-PCM. *Sol Energy* 2019;177:178–91.
- [55] Aspen HYSYS V9. 2017, <https://www.aspentech.com/en>.
- [56] Ebrahimi-Moghadam A, Farzaneh-Gord M. Optimal operation of a multi-generation district energy hub based on electrical, heating, and cooling demands and hydrogen production. *Appl Energy* 2022;309:118453.
- [57] Shamsim M, Rooeentan S, karami B, Elyasi Gomari K, Naseri M, Bonyadi M. Design and thermodynamic analysis of a novel structure utilizing coke oven gas for LNG and power cogeneration. *Energy* 2023;277:127656.
- [58] Löffler G, Sieber R, Harasek M, Hofbauer H, Hauss R, Landauf J. NOx formation in natural gas combustion—a new simplified reaction scheme for CFD calculations. *Fuel* 2006;85:513–23.
- [59] Lienhard JH, Lienhard VJH. *A heat transfer textbook*. third ed.. Cambridge, Massachusetts: Phlogiston Press; 2003.

- [60] Solidworks. Solidworks flow simulation 2018: technical reference. Waltham: Solidworks Corporation; 2018.
- [61] Wang Z, Zhu M, Zhang H, Zhou Y, Sun X, Dou B, et al. Experimental and simulation study on the heat transfer mechanism and heat storage performance of copper metal foam composite paraffin wax during melting process. *Energy* 2023;272:127167.
- [62] Lin W, Ling Z, Fang X, Zhang Z. Experimental and numerical research on thermal performance of a novel thermal energy storage unit with phase change material. *Appl Therm Eng* 2021;186:116493.
- [63] Loprete J, Trojanowski R, Butcher T, Longtin J, Assanis D. Enabling residential heating decarbonization through hydronic low-temperature thermal distribution using forced-air assistive devices. *Appl Energy* 2024;353:122031.
- [64] Bellos E, Tzivanidis C, Papadopoulos A. Optical and thermal analysis of a linear fresnel reflector operating with thermal oil, molten salt and liquid sodium. *Appl Therm Eng* 2018;133:70–80.
- [65] Demissie Tegenaw P, Gebreslasie Gebrehiwot M, Vanierschot M. On the comparison between computational fluid dynamics (CFD) and lumped capacitance modeling for the simulation of transient heat transfer in solar dryers. *Sol Energy* 2019;184:417–25.
- [66] Thermal properties of some building and insulation materials. <http://materias.fi.uba.ar/6731/Tablas/Tabla6.pdf>.
- [67] Vaxasoftware. http://www.vaxasoftware.com/doc_edu/fis/calorespec.pdf.
- [68] PMC PARABOLA. <https://www.palabora.com/Our-Activities/Our-products/Vermiculite/Vermiculite-specifications>.
- [69] Reddy KS, Ravi Kumar K. Estimation of convective and radiative heat losses from an inverted trapezoidal cavity receiver of solar linear Fresnel reflector system. *Int J Therm Sci* 2014;80:48–57.
- [70] IGMO. Iberian Gas Market Operator. <https://www.mibgas.es/en>.
- [71] Villafior G, Morales GV, Velasco J. Significant variables in the combustion process of natural gas. *Información Tecnológica* 2008;19(4):57–62.
- [72] Sun MMin, Ma Z. Effects of heat-treatment and hot-dip galvanizing on mechanical properties of RHS. *J Constr Steel Res* 2019;153:603–17.
- [73] Jugjai S, Rungsimuntuchart N. High efficiency heat-recirculating domestic gas burners. *Exp Therm Fluid Sci* 2002;26:581–92.
- [74] IEA. Net Zero by 2050: A roadmap for the global energy sector. <https://www.iea.org/reports/net-zero-by-2050>.
- [75] Tianjin Gongda Galvanizing Equipment Co., Ltd. <http://gd-galvanize.com/2-1-electric-ceramic-immersion-heaters/178431/>.
- [76] Mu L, Wang S, Lu J, Li C, Lan Y, Liu G, et al. Effect of hydrogen-enriched natural gas on flue gas waste heat recovery potential and condensing heat exchanger performance. *Energy* 2024;286:129591.
- [77] Kakir Erdener B, Sergi B, Guerra OJ, Lazaro Chueca A, Pambour K, Brancucci C, et al. A review of technical and regulatory limits for hydrogen blending in natural gas pipelines. *Int J Hydrog Energy* 2023;48:5595–617.
- [78] Du W, Zhou S, Qiu H, Zhao J, Fan Y. Experiment and numerical study of the combustion behavior of hydrogen-blended natural gas in swirl burners. *Case Stud Therm Eng* 2022;39:102468.
- [79] Kashir B, Tabejamaat S, Jalalatin N. A numerical study on combustion characteristics of blended methane-hydrogen bluff-body stabilized swirl diffusion flames. *Int J Hydrog Energy* 2015;40:6243–58.
- [80] Deymi-Dashtebayaz M, Ebrahimi-Moghadam A, Pishbin SI, Pourramezan M. Investigating the effect of hydrogen injection on natural gas thermo-physical properties with various compositions. *Energy* 2019;167:235–45.
- [81] EU European Commission. Energy efficiency directive (2012/27/EU). 2012.
- [82] Guelpa E, Bischi A, Verda V, Chertkov M, Lund H. Towards future infrastructures for sustainable multi-energy systems: A review. *Energy* 2019;184:2–21.
- [83] European Parliament and the Council. Directive 2004/8/EC on the promotion of cogeneration based on the useful heat demand in the internal energy market. 2004.
- [84] Jamora JB, Gudia SEL, Woo Go A, Giduquio MB, Orilla JWA, Loretero ME. Potential reduction of greenhouse gas emission through the use of sugarcane ash in cement-based industries: A case in the Philippines. *J Clean Prod* 2019;239:118072.
- [85] Hepbasli A, Ozalp N. Co-generation studies in Turkey: an application of a ceramic factory in Izmir, Turkey. *Appl Therm Eng* 2002;22:679–91.
- [86] Barasa Kabeyi MJ, Akanni Olanrewaju O. Cogeneration potential of an operating diesel engine power plant. *Energy Rep* 2022;8:744–54.
- [87] Wang Y, Yu L, Nazir B, Zhang L, Rahmani H. Innovative geothermal-based power and cooling cogeneration system; thermodynamic analysis and optimization. *Sustain Energy Technol Assess* 2021;44:101070.
- [88] Chantasiriwan S. The improvement of energy efficiency of cogeneration system by replacing desuperheater with steam–air preheater. *Energy Rep* 2020;6:752–7.
- [89] Katsigiannis P, Papadopoulos D. A general technoeconomic and environmental procedure for assessment of small-scale cogeneration scheme installations: Application to a local industry operating in Thrace, Greece, using microturbines. *Energy Convers Manage* 2005;46:3150–74.
- [90] Bartela Ł, Kotowicz J, Dubiel-Jurgas K. Investment risk for biomass integrated gasification combined heat and power unit with an internal combustion engine and a stirling engine. *Energy* 2018;150:601–16.
- [91] Thombare D, Verma S. Technological development in the Stirling cycle engines. *Renew Sustain Energy Rev* 2008;12:1–38.
- [92] Zare S, Tavakolpour-Saleh A, Sangdani M. Investigating limit cycle in a free piston Stirling engine using describing function technique and genetic algorithm. *Energy Convers Manage* 2020;210:112706.
- [93] Valenti G, Campanari S, Silva P, Ravidà A, Macchi E, Bischi A. On-off cyclic testing of a micro-cogeneration Stirling unit. *Energy Procedia* 2015;75:1197–201.
- [94] Vannoni C, Battisti R, Drigo S. Potential for solar heat in industrial processes, solar heating and cooling executive committee of the international energy agency. IEA; 2008.
- [95] Imran Ismail M, Alafiza Yunus N, Hashim H. Integration of solar heating systems for low-temperature heat demand in food processing industry – A review. *Renew Sustain Energy Rev* 2021;147:111192.
- [96] Karim MA, Hawlader MNA. Development of solar air collectors for drying applications. *Energy Convers Manage* 2004;45:329–44.
- [97] Hisan Farjana S, Huda N, Parvez Mahmud MA, Saidur R. Solar process heat in industrial systems – A global review. *Renew Sustain Energy Rev* 2018;82:2270–86.